# Kinetics and Mass Yields of Aqueous Secondary Organic Aerosol from Highly Substituted Phenols Reacting with a Triplet Excited State

Lan Ma<sup>1</sup>, Chrystal Guzman<sup>1</sup>, Christopher Niedek<sup>2</sup>, Theodore Tran<sup>1</sup>, Qi Zhang<sup>2</sup>, and Cort

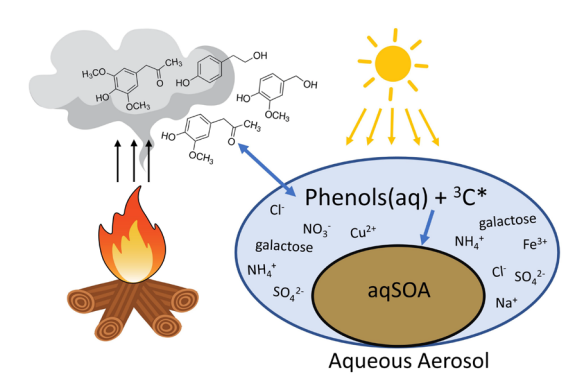
Anastasio<sup>1</sup>\*

<sup>1</sup>Department of Land, Air, and Water Resource, University of California, Davis, CA 95616

<sup>2</sup>Department of Environmental Toxicology, University of California, Davis, CA 95616

Correspondence to: Cort Anastasio (<u>canastasio@ucdavis.edu</u>)

# 1 TOC Abstract Art



## **ABSTRACT**

4

5 Biomass burning emits large amounts of phenols, which can partition into cloud/fog drops and aerosol 6 liquid water (ALW) and react to form aqueous secondary organic aerosol (aqSOA). Triplet excited states 7 of organic compounds (<sup>3</sup>C\*) are a likely oxidant, but there are no rate constants with highly substituted 8 phenols that have high Henry's law constants  $(K_{\rm H})$  and are likely important in ALW. To address this gap, 9 we investigated the kinetics of six highly substituted phenols with the triplet excited state of 3,4dimethoxybenzaldehyde. Second-order rate constants at pH 2 are all fast, (2.6 - 4.6) ×10<sup>9</sup> M<sup>-1</sup>s<sup>-1</sup>, while 10 11 values at pH 5 are 2 to 5 times smaller. Rate constants are reasonably described by a quantitative 12 structure-activity relationship with phenol oxidation potentials, allowing rate constants of other phenols to 13 be predicted. Triplet-phenol kinetics are unaffected by ammonium sulfate, sodium chloride, galactose (a 14 biomass-burning sugar), or Fe(III). In contrast, ammonium nitrate increases the rate of phenol loss by 15 making hydroxyl radical, while Cu(II) inhibits phenol decay. Mass yields of aqueous SOA from triplet 16 reactions are large and range from 59 to 99%. Calculations using our data along with previous oxidant 17 measurements indicate that phenols with high  $K_{\rm H}$  can be an important source of aqSOA in ALW, with 18 <sup>3</sup>C\* typically the dominant oxidant.

19

20

21

22

23

24

25

26

27

#### INTRODUCTION

Airborne particulate matter (PM) impacts human health, visibility and climate.<sup>1–3</sup> One of the major components of PM is secondary organic aerosol (SOA), which is formed by oxidation of volatile organic compounds in the gas phase followed with condensation, as well as in cloud/fog drops and possibly aerosol liquid water (ALW).<sup>4–6</sup> Biomass burning (BB) is a major source of PM<sup>7</sup> and releases large amounts of soluble, reactive gases that can form SOA.<sup>8</sup> One major class of these gases is phenols, which are emitted from the combustion of lignin, with an estimated global source strength of 4.7 Tg yr<sup>-1,9–12</sup> Three of the most abundant phenols emitted from BB are phenol (C<sub>6</sub>H<sub>5</sub>OH or PhOH), guaiacol (2-methoxyphenol), and

syringol (2,6-dimethoxyphenol), which represent the base structures of BB phenols. 10,11 Besides being 28 oxidized in the gas phase, these three species have moderate Henry's Law constants ( $K_{\rm H} = 10^3 - 10^4 \, {\rm M}$ 29 atm<sup>-1</sup> at 278 K), <sup>13–15</sup> enabling them to partition into cloud/fog drops where they can react with a number of 30 aqueous oxidants to form aqSOA. 6,16-19 31 32 Triplet excited states of organic compounds (<sup>3</sup>C\*) are a class of aqueous oxidants that are formed when light-absorbing organics (i.e., brown carbon) absorb sunlight. <sup>20</sup> Triplets can react with gas-phase alkenes to 33 make additional PM mass at the surface of particles, 21,22 convert glyoxal into highly oxygenated 34 35 compounds,<sup>23,24</sup> and oxidize SO<sub>2</sub> to sulfate.<sup>25</sup> While hydroxyl radical (•OH) is often considered the dominant oxidant for aqSOA formation, <sup>26</sup> triplets can be an important oxidant in fog and cloud water, in 36 part because their concentrations are typically 10 - 100 times higher than OH.27 Moreover, triplet 37 concentrations appear to be enhanced by a few orders of magnitude in aerosol water,28 indicating a 38 potentially major role in agSOA formation in ALW. 39 40 Simple phenols react with triplets with rate constants near diffusion-controlled, and also react rapidly with OH, 16,19,29 giving aqueous lifetimes of a few hours, comparable to gas-phase lifetimes. 14,19 These phenol-41 triplet reactions also efficiently form aqSOA, with mass yields in the range of 70 – 120%. 16,19,30 Compared 42 with OH oxidation in the gas phase, aqueous reactions in cloud/fog drops can dominate the formation of 43 phenolic SOA. 16,19 44 45 While a number of studies have investigated aqSOA formation under cloud and fog water conditions, less is known about SOA formation in ALW.31-33 ALW is ubiquitous, with a mass often equivalent to (or greater 46 than) the dry particle mass, 34 but the amount of particle water (typically  $1 - 100 \mu g \text{ m}^{-3}$ ) is orders of 47 magnitude lower than that of fog/cloud drops.<sup>5,35</sup> Because of this, ALW contains very high concentrations 48 of organic and inorganic species, which might affect reaction kinetics, including for aqSOA formation. 31,36-49 38 50

The low water content of ALW leads to very limited partitioning of s	simple phenols to particle water; e.g.
less than 0.001% of syringol will partition into the water phase for	an ALW content of 100 $\mu g$ m <sup>-3</sup> , ar
approximate upper bound for a wintertime aerosol in California's	Central Valley. <sup>38</sup> In contrast, highly
substituted phenols have much higher $K_{\rm H}$ values and might be signifi-	cant sources of aqSOA in ALW. For
example, for the six BB phenols in Figure 1,9-11,39-41 Henry's law cor	nstants range from 10 <sup>6</sup> to 10 <sup>9</sup> M atm
at 278 K,15 corresponding to aqueous fractions of 2 to 58% for an AL	W content of $100 \mu\mathrm{g}$ m <sup>-3</sup> . In addition
the highly substituted phenols measured by Schauer et al. are abundar	nt, together accounting for roughly 30
- 45% of total phenols emitted from wood burning. 10 Thus highly	y substituted phenols should be the
dominant phenols in ALW, present at much higher levels than simple	e phenols. Despite this, the reactions
of highly substituted phenols with triplet excited states to make aqSO	OA have not been examined and it is
unclear whether the high solute concentrations in ALW affect these k	inetics.
To assess the potential significance of these six highly substituted phe	enols as sources of aqSOA in ALW,
we measure their rate constants with the triplet state of 3,4-dimethoxy	benzaldehyde (DMB), which is
present in biomass burning particles <sup>42</sup> and has a reactivity similar to a	ambient triplets in fog and PM in
regions of significant wood combustion. <sup>27,28</sup> We also examine the imp	pacts of molar concentrations of salts
and a cellulose-derived sugar, and trace amounts of transition metal ic	ons, on the triplet kinetics. We then
determine SOA mass yields from these reactions and develop a quant	itative structure-activity relationship
between phenol oxidation potentials and second-order rate constants	with the DMB triplet state. Finally,
we calculate the gas- and aqueous-SOA formation rates for three mod	del phenols to investigate their
significance as sources of aqSOA and the dependence of this chemist	

# MATERIALS AND METHODS

# **Chemicals and Solutions**

74 Chemicals were used as received. 3,4-dimethoxybenzaldehyde (DMB) (99%), 4-hydroxy-3methoxyphenylacetone (GA) (96%), 2-(4-hydroxyphenyl)ethanol (TYR) (98%), vanillyl alcohol (VAL) 75 76  $(\ge 98\%)$ , trans-ferulic acid (FA) (99%), syringic acid (SyrAcid) ( $\ge 95\%$ ), 2-nitrobenzaldehyde (2-NB) 77 (98%), galactose ( $\geq$  98%), ammonium sulfate ( $\geq$  99%), ammonium nitrate ( $\geq$  99%), Copper(II) sulfate 78 pentahydrate ( $\geq 98\%$ ), Iron(III) chloride ( $\geq 97\%$ ), and sodium chloride ( $\geq 99\%$ ) were from Sigma-79 Aldrich. (3,5-Dimethoxy-4-hydroxyphenyl)acetone (syringyl acetone, SA) (82%) was synthesized by 80 Carbosynth LLC. Sodium borate (ACS grade) and sulfuric acid (trace metal grade) were from Fisher 81 Scientific. All chemical solutions were prepared using air-saturated ultrapure water (Milli-Q water) from 82 a Milli-Q Advantage A10 system (Millipore; ≥18.2 MΩ cm) with an upstream Barnstead activated carbon 83 cartridge. 84 Kinetic solutions contained 5 – 100  $\mu$ M of one phenol (ArOH), 10  $\mu$ M DMB, and either sulfuric acid or 85 sodium borate to adjust pH to 2 or 5, respectively. In this work, we use the abbreviation "PhOH" to 86 represent the compound phenol (C<sub>6</sub>H<sub>5</sub>OH), and the terms "phenol(s)" and "ArOH" to represent phenols 87 more generally. 88

## **Solution Illumination and Chemical Analysis**

89

90

91

92

93

94

95

96

Air-saturated solutions were illuminated in a stirred, airtight quartz cell (2-cm path length) (Spectrocell) at 20 °C. Samples were illuminated with a 1000 W Xenon arc lamp with a water filter, an AM1.0 air mass filter (AM1D-3L, Sciencetech), and a 295-nm long-pass filter (20CGA-295, Thorlabs) to simulate tropospheric sunlight. Dark control samples were wrapped in aluminum foil and kept in the same photoreactor chamber at 20 °C.

During illumination, aliquots were periodically removed from the illuminated and dark cells to measure concentrations of ArOH and DMB with HPLC (Supporting Information Table S1). Each experiment day

- 97 the photon flux was determined by measuring the photolysis rate constant ( $j_{2NB,exp}$ ) of a 10  $\mu$ M 2-
- 98 nitrobenzaldehyde (2NB) solution in a quartz cell identical to that used to illuminate the phenol solution.

#### Kinetic Analysis

99

111

- The full description of the kinetic analysis is in Smith  $et\ al.^{19}$  and only an abbreviated version is given here.
- The measured pseudo-first-order rate constant for phenol loss ( $k'_{Light}$ ) was determined as the negative of the
- slope from a linear fitting of ln([ArOH]<sub>1</sub>/[ArOH]<sub>0</sub>) versus illumination time, where [ArOH] is the
- 103 concentration of phenol (at time zero or time t). Values of  $k'_{\text{Light}}$  were normalized to sunlight conditions at
- midday on the winter solstice at Davis (solar zenith =  $62^{\circ}$ ;  $j_{2NB,win} = 0.0070 \text{ s}^{-1}$ )<sup>43</sup> and corrected for internal
- light screening:

$$k'_{\text{ArOH}} = \left[ \frac{k'_{\text{Light}}}{S_{\lambda} \times j_{2\text{NB,exp}}} \right] \times j_{2\text{NB,win}}$$
 (1)

- where  $k'_{ArOH}$  is the normalized first-order rate constant,  $S_{\lambda}$  is the internal light screening factor, and  $j_{2NB,exp}$  is the measured rate constant of 2NB loss. Protonated  ${}^{3}DMB^{*}$  (HT) has a p $K_{a}$  of 3.3 and a higher reactivity than its neutral form (T). Therefore, we performed kinetic experiments at pH 2 (where 95% of  ${}^{3}DMB^{*}$  is in the protonated form and the apparent first-order rate constant for phenol loss ( $k'_{ArOH}$ ) is essentially  $k'_{HT}$ )
- 112 As described in Smith *et al.*, <sup>19</sup> the rate constant of phenol loss is a function of the triplet source and sinks:

and pH 5 (where the neutral form represents 98% of  ${}^{3}DMB^{*}$  and  $k'_{ArOH}$  is equal to  $k'_{T}$ ).

113 
$$k'_{ArOH} = \frac{1}{\left(\frac{k_{O2+3DMB*}[O_2] + k'_{3DMB*}}{j_{hv,abs}\Phi_{\rm ISC}[DMB] \times k_{ArOH+3DMB*}} + \frac{k_{ArOH+3DMB*} + k_Q}{j_{hv,abs}\Phi_{\rm ISC}[DMB] \times k_{ArOH+3DMB*}} [ArOH]\right)}$$
(2)

Here,  $k_{O2+3DMB^*}$  is the bimolecular rate constant for reaction of  ${}^3DMB^*$  with dissolved  $O_2$ ,  $k'{}_{3DMB^*}$  is the first-order rate constant for relaxation of  ${}^3DMB^*$  to the ground state,  $j_{hv,abs}$  is the rate constant for light absorption by DMB under Davis winter solstice conditions,  $\Phi_{ISC}$  is the intersystem crossing quantum yield, [DMB] is the concentration of DMB,  $k_{ArOH+3DMB^*}$  is the second-order rate constant for ArOH reacting with

 $^{3}$ DMB\*, and  $k_{0}$  is the second-order rate constant for quenching of  $^{3}$ DMB\* by ArOH without loss of ArOH.

Equation 2 can be simplified and inverted to:

$$\frac{1}{k'_{ArOH}} = a + b[ArOH] \tag{3}$$

To determine  $k_{ArOH+3DMB^*}$ , we fitted our data of  $k'_{ArOH}$  versus [ArOH] to this equation to obtain values of a

and b, and then used measured or estimated values for the other parameters in Eq. 2 (see Table S2) to

calculate  $k_{ArOH+3DMB}*$ .

To test if phenols undergo significant direct photodegradation, solutions containing 5 – 100  $\mu$ M of one

phenol were illuminated in the absence of DMB. For the three phenols with direct photodegradation (FA,

SyrAcid, SA), we corrected their first-order rate constants with <sup>3</sup>DMB\* by determining the rate constants

for photodecay and subtracting these contributions from the triplet results (Section S1).

## SOA Mass Yields $(Y_{SOA})$

aqSOA mass yields were determined by illuminating a solution containing  $100 \,\mu\text{M}$  phenol and  $10 \,\mu\text{M}$  DMB at pH 5 until approximately 88% of the phenol had reacted (i.e., until three half-lives was reached). For phenols with direct photodegradation, we instead used  $50 \,\mu\text{M}$  phenol and  $10 \,\mu\text{M}$  DMB. Aliquots were taken at time zero and at one, two, and three phenol half-lives (i.e.  $t_{1/2}$ ,  $2t_{1/2}$ , and  $3t_{1/2}$ ) and were analyzed by HPLC and High Resolution Time-of-Flight Aerosol Mass Spectrometry (HR-ToF-AMS).  $^{17,30,44}$  Prior to AMS analysis, samples were spiked with known amounts of ammonium sulfate as an internal standard and were atomized using a constant output atomizer (TSI, Model 3076) with argon as the carrier gas. The resulting aerosol was then dried in a diffusion drier before being sampled in the AMS. The evaporation of semi-volatile compounds during the aerosolization and drying process will not introduce significant biases in aqSOA mass yield analysis based on previous studies.  $^{17,30}$  Mass spectra up to m/z 400 were acquired. Each sample was run twice on AMS and data were analyzed using the standard analysis software (SQUIRREL v1.62F and PIKA v1.22F).  $^{17,30}$  The SOA mass concentration was calculated from the measured organic

mass after subtracting the contribution from the unevaporated phenol precursor. The aqSOA mass yield in each sample was calculated by:

$$Y_{SOA} = \frac{SOA \ mass \ formed}{mass \ of \ phenol \ reacted} \tag{4}$$

More details are provided in the Supporting Information Section S2.

#### **Oxidation Potentials**

We determined oxidation potentials for the loss of one electron for the six phenols studied here (Figure 1) as well as for PhOH, guaiacol, syringol, catechol, hydroquinone, and resorcinol. Values were both measured by cyclic voltammetry (CV) and computed using Gaussian; details are in Supporting Information Section S3.

#### **RESULTS AND DISCUSSION**

#### Oxidation Kinetics of Phenols by the Triplet Excited State of DMB

To determine the second-order rate constant for a phenol with  ${}^{3}DMB^{*}$ , we measure the first-order phenol decay rate constant ( $k'_{ArOH}$ ) as a function of initial phenol concentration at pH 2 and 5. In illuminated samples, all phenols follow pseudo-first-order decay (e.g., Figure S2) and the loss of DMB is insignificant (less than 5%). In dark controls there is no significant loss of phenol or DMB. GA, TYR, and VAL show negligible direct photodegradation over our illumination periods, while direct photodegradation of FA, SA, and SyrAcid contributes 3% – 34% of the phenol loss measured in the presence of DMB; we correct for this loss in our calculations of the triplet rate constants (Section S1). In addition, *trans*-FA undergoes photoisomerization to form *cis*-FA, reaching a photostationary state of the two isomers within 10 min of illumination (see Section S4 of the Supporting Information). As shown in Figure S2, GA decay at 5 °C is

not statistically different from that at 20  $^{\circ}$ C, indicating no significant temperature dependence of the triplet-phenol reactions, consistent with past work. <sup>19</sup>

The apparent first-order decay rate constant of phenols with  ${}^{3}\text{DMB*}$  ( $k'_{ArOH}$ ), which is the product of the second-order rate constant for phenol with  ${}^{3}\text{DMB*}$  ( $k_{ArOH+3DMB*}$ ) and [ ${}^{3}\text{DMB*}$ ], decreases with increasing initial phenol concentration (Figure S5). This is because a higher phenol concentration increases the sink for  ${}^{3}\text{DMB*}$ , reducing the triplet steady-state concentration. Thus  $1/k'_{ArOH}$  increases with increasing phenol concentration. Equation 3 is used to fit these data (Figure S5) to obtain the regression parameters (Table S3), and then  $k_{ArOH+3DMB*}$  is derived from Equation 2 with parameters shown in Table S2.

Measured second-order rate constants for reactions of phenols with  ${}^{3}DMB^{*}$  are shown in Figure 2 and Table S4. The rate constants are all rapid, especially at pH 2 where values of  $k_{ArOH+HT}$  are in the range of (2.6 – 4.6) × 10<sup>9</sup> M<sup>-1</sup> s<sup>-1</sup>. At pH 5, corresponding values of  $k_{ArOH+T}$  are 1.6 to 5.4 times lower and more variable among phenols, with a range of (0.29 – 2.7) ×10<sup>9</sup> M<sup>-1</sup> s<sup>-1</sup>, showing that the protonated form of  ${}^{3}DMB^{*}$  (p $K_{a}$  3.3) is more reactive than its neutral form.  ${}^{19,20}$  TYR (a derivative of PhOH) has the slowest rate constant with  ${}^{3}DMB^{*}$ , while SA (a derivative of syringol, i.e., 2,6-dimethoxyphenol) has the highest rate constant among our six phenols. These results are consistent with previous findings that methoxy substitution enhances rate constants by donating electron density to the aromatic ring, activating the phenol.  ${}^{19,45}$ 

Phenolic hydroxyl groups typically have  $pK_a$  values around 10.<sup>46</sup> Therefore, for the phenols we studied (Figure 1), there is no significant deprotonation of the phenolic hydrogen and the compounds are in the neutral form at both pH 2 and pH 5. However, FA and SyrAcid also have carboxylic acid groups, which have  $pK_a$  values of 4.6 and 4.2, respectively.<sup>47</sup> At pH 2, the mole fractions for the neutral forms of FA (HFA) and SyrAcid (SyrCOOH) are greater than 99%. However, at pH 5, FA and SyrAcid will mostly dissociate so that the neutral forms are minor and more than 70% of each species is present as the conjugate base (FA<sup>-</sup> or SyrCOO<sup>-</sup>). Therefore, the apparent first-order reaction rate constants of FA and SyrAcid with  $^3$ DMB\* at pH 5 represent the reactivity of a mixture of the neutral and ion (carboxylate) forms of the phenols. Through these first-order rate constants, we calculate the second-order rate constants for the neutral and ion forms

(Section S5). At pH 5, the rate constants of the FA<sup>-</sup> isomers are statistically indistinguishable from zero  $(0.31~(\pm~0.36)\times10^9~M^{-1}s^{-1}$  for trans-FA and  $0.29~(\pm~0.36)\times10^9~M^{-1}s^{-1}$  for cis-FA), while the rate constant for HFA is rapid,  $2.1~(\pm~0.54)\times10^9~M^{-1}s^{-1}$  for both isomers. For syringic acid the reactivities of the neutral and carboxylate forms at pH 5 are statistically indistinguishable:  $2.2~(\pm~0.64)\times10^9~M^{-1}s^{-1}$  for SyrCOO-and  $1.8~(\pm~0.44)\times10^9~M^{-1}s^{-1}$  for SyrCOOH.

We also use the fitted regression parameter 'b' in Equation 3 to determine the fraction of phenol interacting with <sup>3</sup>DMB\* that leads to reaction (i.e., oxidation of phenol to form products) rather than quenching <sup>3</sup>DMB\* without phenol loss:

$$f_{reaction} = \frac{k_{ArOH+3DMB*}}{k_{ArOH+3DMB*} + k_Q} = \frac{1}{b \times j_{hv,DMB} \Phi_{ISC}[DMB]}$$
(6)

Values of  $k_Q$  are calculated from parameters 'a' and 'b' and are shown in Table S4. For most of our six phenols,  $k_Q$  has the same order of magnitude as  $k_{ArOH+3DMB^*}$ , which is consistent with past work on methylphenols and methoxyphenols with other triplets. <sup>16,48</sup> The range of  $f_{reaction}$  values for our phenols is 0.20-0.88 at pH 2 and 0.09-0.98 at pH 5 (Table S4). For all of the phenols except for SA,  $f_{reaction}$  at pH 2 is higher than that at pH 5, by an average factor of 2.9. For TYR at pH 5, which has a slow rate constant of oxidation by <sup>3</sup>DMB\*, the reaction fraction is only 0.09, i.e., 91% of the TYR - <sup>3</sup>DMB\* interaction leads to <sup>3</sup>DMB\* quenching but not TYR loss. This result is similar to other research, which observed that PhOH ( $C_6H_5OH$ ) at pH 8 has an oxidation rate about ten times lower than the quenching rate with triplet. <sup>48</sup> There are at least two mechanisms by which the <sup>3</sup>DMB\*-phenol interaction could lead to no phenol loss. One possibility is that the triplet oxidizes the phenol to make a phenoxyl radical, but then this radical is reduced (e.g., by superoxide or hydroperoxyl radical) to regenerate the parent phenol, resulting in no apparent reaction. <sup>48,49</sup> In the case of FA, where  $f_{reaction}$  is low ( $\leq$ 0.20) we suspect that another mechanism is important: energy transfer from <sup>3</sup>DMB\* resulting in reversible isomerization of FA. This is what occurs between triplets and sorbic acid, <sup>50</sup> with the resulting isomerization used as a probe to quantify triplet concentrations. <sup>50,51</sup>

## aqSOA Mass Yields

Aqueous triplet reactions of simple phenols (e.g., PhOH, guaiacol, and syringol) efficiently form low-volatility products, with significant aqSOA yields. <sup>16,19,30</sup> Here we investigate whether triplet reactions with highly-substituted phenols (Figure 1) also produce significant amounts of aqSOA, by illuminating solutions containing a phenol and DMB and measuring the aqSOA mass with AMS.

Figure S6 shows the SOA mass yields at one, two, and three half-lives for each phenol, i.e., after 50%, 75%, and 88% of the initial phenol has reacted. For a given compound, the yields are typically very similar at all three time points and between duplicates, so for each phenol we calculated the average mass yield from all six data points, except for FA, where an outlier was removed. As shown in Figure 3, aqSOA mass yields are generally high, in the range of 59% - 99%, and with an overall average ( $\pm 1 \sigma$ ) of 83 ( $\pm 14$ )%. This result is comparable to the results in Smith *et al.*, where aqSOA mass yields from PhOH, guaiacol and syringol reacting with  $^3$ DMB\* are near 100%. These aqueous yields are significantly higher than  $Y_{SOA}$  values from gaseous phenol reactions with  $^4$ OH, which are in the range of 10 - 50%.  $^{52,53}$  An early step in the aqueous triplet oxidation of a phenol forms phenoxyl radicals, which couple to produce low volatility oligomers,  $^{30,44,48}$  in contrast to gas-phase reactions with  $^4$ OH, which favor fragmentation of aromatic rings to form more volatile products.  $^{30,52}$ 

## **Effect of Solutes**

Unlike relatively dilute cloud or fog drops, particle water typically contains very high concentrations of inorganic and organic solutes, with ionic strengths typically of several molar. <sup>38,54,55</sup> The high ionic strength in ALW might affect triplet kinetics, based on past work showing that seawater concentrations of halides inhibit electron transfer of triplet excited states of natural organic matter. <sup>56,57</sup> However, the effect of ALW-relevant solutes on triplet kinetics has been largely overlooked. Ammonium nitrate, ammonium sulfate, and sodium chloride are common salts in atmospheric aerosols, as are cellulose-derived sugars from biomass

burning such as levoglucosan and galactose (a hydrolyzed isomer of levoglucosan). 58 Also, transition metal ions, Fe(III) and Cu(II), can be important drivers of atmospheric aqueous chemistry through redox cycling.<sup>59</sup> Dissolved Fe concentrations vary from 10<sup>-9</sup> to 10<sup>-4</sup> µM in cloud/fog water, while copper concentrations are generally 10 times lower.<sup>60</sup> Their concentrations are enhanced in aerosol water but little is known of their effects on triplet kinetics. To study the impacts of these solutes and metals on triplet kinetics, we illuminated solutions containing 10  $\mu$ M GA (the model phenol), 10  $\mu$ M DMB, and varying concentrations of one solute or metal, and determined the pseudo-first-order rate constant of GA decay  $(k'_{GA})$ . The ratio of the GA decay rate constant with solute addition to the rate constant without solute (i.e., the ratio  $k'_{GA,solute}/k'_{GA,0}$ ) was then calculated. As shown in Figure 4, 0.5 M ammonium nitrate increases the rate constant for GA loss significantly, by a factor of over 20 compared with no NH<sub>4</sub>NO<sub>3</sub> (after correction for light screening by ammonium nitrate). The DMB loss rate also increases with higher concentrations of NH<sub>4</sub>NO<sub>3</sub> (Figure S7). These impacts are because NO<sub>3</sub><sup>-</sup> photolysis forms OH, 61,62 which reacts with GA and DMB. To determine if ionic strength makes any contribution to the enhanced decay rate constant in the presence of salts, we next used ammonium sulfate and sodium chloride, which don't undergo photolysis to form reactive species. As shown in Figure 4, a high concentration of ammonium sulfate or sodium chloride has only a small, and statistically insignificant, impact on triplet kinetics. There is a tendency that 2 M of these salts increases the rate constant for GA loss, which might be due to the high salt concentration decreasing the solubility of dissolved oxygen.<sup>63</sup> Since oxygen is the dominant scavenger for <sup>3</sup>DMB\* in these solutions, decreasing the dissolved O<sub>2</sub> concentration will increase the steady-state concentration of <sup>3</sup>DMB\*, resulting in a higher GA decay rate. For example, 2 M NaCl decreases O<sub>2</sub> solubility by around 40%, <sup>64</sup> which is roughly consistent with the increased k'GA at pH 2. Zhou et al. found that acetosyringone direct photodegradation increased by

a factor of roughly six in the presence of 2 M NaClO<sub>4</sub>. <sup>37</sup> If GA direct photodegradation was enhanced by a

similar factor in our (NH<sub>4</sub>)<sub>2</sub>SO<sub>4</sub> and NaCl solutions, it would still be a minor sink, contributing less than 5%

of total GA decay in the presence of <sup>3</sup>DMB\*, indicating that GA direct photodegradation does not affect

235

236

237

238

239

240

241

242

243

244

245

246

247

248

249

250

251

252

253

254

255

256

257

258

our results significantly. Addition of 0.9 M galactose also causes no significant change to the rate constant
for GA decay. Figure S8 shows the dependence of $k'_{\rm GA}$ on the concentration of galactose. The consistency
of these rate constants indicates that galactose reacts, at most, only very slowly with <sup>3</sup> DMB*; otherwise,
high concentrations of galactose would suppress the <sup>3</sup> DMB* concentration, leading to a slower GA decay.
From our kinetic data in Figure 4 we can estimate an upper-bound for the rate constant of galactose with
$^3 DMB^*$ , by assuming that we cannot discern a $2\sigma$ decrease in the average $k'_{GA}$ at the highest galactose
concentration (0.9 M). Applying this assumption to our data gives a value for $k_{\rm galactose+3DMB}$ * of $\leq 1 \times 10^5$ M
$^{1}\mathrm{s}^{\text{-1}}$ at pH 2 and 5 and suggests that cellulose-derived sugars are insignificant sinks for triplets in the ALW
of biomass-burning particles.
Adding Fe(III) increases the overall decay rate of GA because photolysis of iron complexes Fe(OH) <sup>2+</sup> and
FeCl <sup>2+</sup> forms *OH and Cl*, which react with GA. <sup>65-67</sup> Figure S9 shows GA decay in the presence of Fe(III)
during illumination and the contribution of Fe chemistry. After subtracting the contribution of photolysis
of Fe(III), the GA decay rate by <sup>3</sup> DMB* is not statistically different in the presence of Fe(III) (Figure 4). In
contrast, Cu(II) strongly inhibits the decay of GA (Figure 4). Pan et al. observed the same inhibition by
Cu(II) on the decay of phenolic compounds by triplets. <sup>68,69</sup> They proposed that Cu(II) is photochemically
reduced to Cu(I),70 which reacts with phenoxyl radicals to regenerate the parent phenol, slowing phenol
decay. <sup>68</sup> As shown in Figure 4, inhibition of GA loss by Cu(II) is more significant at pH 5 than at pH 2,
likely because of the acid-base speciation of HO <sub>2</sub> • and its conjugate base •O <sub>2</sub> HO <sub>2</sub> • has a pKa of 4.8, <sup>71</sup> so
at pH 2 $HO_2^{\bullet}$ is the dominant form, but at pH 5 $^{\bullet}O_2^-$ dominates. Both of these $O_2(\text{-I})$ species reduce $Cu(II)$
to $Cu(I)$ , but the reaction with ${}^{\bullet}O_2{}^-$ is around 80 times faster, ${}^{72}$ so we expect a higher $Cu(I)$ concentration at
pH 5 compared to pH 2, leading to stronger inhibition of phenol decay.

# **Quantitative Structure-Activity Relationships**

Since biomass burning emits over 50 phenolic compounds,  $^{9,10,73}$  we would like to develop a quantitative structure-activity relationship (QSAR) to predict rate constants for phenols reacting with triplets. Following promising research on QSARs between reactant oxidation potentials ( $E_{OX}$ ) and their rate constants with triplets,  $^{74-76}$  we pursued a similar approach for phenols with the triplet state of DMB. While there are some measurements of phenol oxidation potentials,  $^{77-79}$  there are no values for the six phenols we studied here (Figure 1). Therefore we both measured and computed  $E_{OX}$  values for our six phenols as well as for the six phenols whose rate constants with  $^{3}$ DMB\* were measured by Smith *et al.*  $^{16,19}$ 

Oxidation potentials of phenols determined in this work are shown in Table S5.  $E_{\rm OX}$  values measured by cyclic voltammetry at pH 5 are lower than that at pH 2, as expected,<sup>79</sup> while computed  $E_{\rm OX}$  values are higher than measured values, consistent with the finding of other groups.<sup>78,80</sup> The correlation between our measured and computed  $E_{\rm OX}$  values is modest ( $r^2 = 0.34$ ; Figure S10), but our measured values are well correlated with values from the literature ( $r^2 = 0.99$ ; Figure S10).

As seen in Figure 5, oxidation potentials correlate well with the log of the second-order rate constants with the DMB triplet: as the oxidation potential increases (i.e., the phenol is more difficult to oxidize), the rate constant generally decreases. Based on  $R^2$  values, modeled oxidation potentials perform better than measured values in the QSAR. For the QSAR based on measured  $E_{OX}$  values at pH 2, most of the phenols are close to the regression line (Figure 5B), but there are two notable outliners, hydroquinone and catechol. The data in the corresponding QSAR at pH 5 are much more scattered. While all of our QSARs are approximately linear in this log-linear space, at lower  $E_{OX}$  values  $k_{ArOH+3DMB}$ \* will plateau as it approaches the diffusion-controlled limit.<sup>48</sup>

#### **ATMOSPHERIC IMPLICATIONS**

Our research group recently showed that concentrations of triplets and singlet molecular oxygen increase by orders of magnitude moving from cloud/fog drops to the more concentrated conditions in aerosol liquid

water, while aqueous hydroxyl radical concentrations decrease.<sup>28</sup> To understand how these changing condensed-phase oxidant conditions alter the formation of SOA from biomass-burning phenols, here we estimate initial rates of SOA formation from three model phenols - syringol (SYR), guaiacyl acetone (GA) and syringyl acetone (SA) - across a range of liquid water contents. In our calculations we assume Henry's law partitioning of the phenols, with  $K_{\rm H}$  values at 278 K of 2.5 × 10<sup>4</sup> M atm<sup>-1</sup> (SYR), 9.1 × 10<sup>6</sup> M atm<sup>-1</sup> (GA), and  $6.1 \times 10^8$  M atm<sup>-1</sup> (SA). We consider reactions with gas-phase OH (at a constant  $1 \times 10^6$ molecules cm<sup>-3</sup>) and aqueous-phase <sup>3</sup>C\*, <sup>1</sup>O<sub>2</sub>\*, and <sup>•</sup>OH, using oxidant concentrations as a function of liquid water content from Figure 5 of Kaur et al. 28 For oxidizing triplet concentrations we use the geometric mean of the two estimates in Kaur et al. Rate constants and SOA mass yields applied in the SOA formation rate calculation are listed in Table S8. We assume an initial particulate matter concentration of 10 µg m<sup>-3</sup>air and that each phenol has an initial total (gas + aqueous) concentration of 5 µg m<sup>-3</sup>-air. Details of the calculations are in SI Section S6. The top row of Figure 6 shows initial SOA formation rates from SYR, GA and SA reacting with each oxidant as a function of LWC from cloud/fog condition (0.33 g m<sup>-3</sup>) to aerosol liquid water (10 µg m<sup>-3</sup>), while the bottom row shows the contribution of each oxidant to aqSOA formation. We start by considering syringol, which has the lowest Henry's law constant of the three phenols here. Under the cloud/fog condition, only about 20% of SYR is present in the aqueous phase (Figure 6A), but the SOA formation rate from aqueous reactions is comparable to that from the gas-phase reaction, and OH is the dominant oxidant in both phases (Figure 6D). When moving to the drier ALW conditions, the fraction of SYR in the aqueous phase decreases rapidly, causing the aqueous \*OH-mediated aqSOA formation rate to drop quickly. Formation of aqSOA by <sup>3</sup>C\* and <sup>1</sup>O<sub>2</sub>\* are initially less sensitive to the decrease in LWC – a result of increasing oxidant concentrations – but they cannot compete with gas-phase OH since so little SYR is in

307

308

309

310

311

312

313

314

315

316

317

318

319

320

321

322

323

324

325

326

327

328

329

the aqueous phase.

The picture is quite different for GA, which has a Henry's law constant that is nearly 400 times higher than SYR. Most GA is in the aqueous phase under cloud/fog conditions, while a negligible amount is aqueous under ALW conditions (Figure 6B). Initially, the decrease in LWC from cloud/fog conditions increases the aqSOA formation rate - even though the aqueous fraction of GA is decreasing - because of the increase in <sup>3</sup>C\* and <sup>1</sup>O<sub>2</sub>\* concentrations. But the aqueous formation of SOA peaks at an LWC of approximately 1 mg m<sup>-3</sup>, and under particle water conditions (100 μg m<sup>-3</sup> and less) gas-phase OH becomes the major source of SOA from GA. The final phenol we consider is syringyl acetone, whose Henry's law constant is roughly 70 times higher than that of GA. Because of this, SA is essentially completely partitioned to the aqueous phase under cloud/fog conditions and even significantly partitioned to the aqueous phase (~ 10%) at an ALW content of 10  $\mu$ g m<sup>-3</sup> (Figure 6C). Coupled with the high  ${}^{3}C^{*}$  and  ${}^{1}O_{2}^{*}$  concentrations under ALW conditions, the result is that aqueous reactions dominate SOA formation throughout the entire range of liquid water contents (Figure 6F). Furthermore, the increase in aqueous oxidant concentrations with decreasing LWC causes the aqSOA formation rate from SA to increase by approximately a factor of 30 as liquid water content drops by a factor of roughly 3000 from cloud/fog conditions to 100  $\mu$ g m<sup>-3</sup> (Figure 6C). While the rate of agSOA formation then falls as LWC continues to drop, the rate at an ALW of 10 µg m<sup>-3</sup> is still around 10 times higher than under cloud conditions. For all three phenols, the contributions of the aqueous oxidants shift as liquid water content decreases from cloud/fog to ALW conditions (Figure 6, bottom row). In the dilute aqueous phase for all three phenols, aqueous OH accounts for roughly 90% of aqSOA formation, 3C\* contributes roughly 10%, and 1O2\* is negligible. Moving toward more concentrated ALW conditions, the aqueous \*OH concentration decreases by a factor of around 6, while  ${}^{1}O_{2}^{*}$  and  ${}^{3}C^{*}$  concentrations initially increase nearly proportionally with particle mass/water ratio and then plateau.<sup>28</sup> Thus the \*OH contribution to aqSOA formation rate decreases as LWC drops, while <sup>1</sup>O<sub>2</sub>\* and <sup>3</sup>C\* become more significant, dominating phenolic aqSOA formation under ALW conditions. As described above, aqueous  ${}^{1}O_{2}^{*}$  and  ${}^{3}C^{*}$  compete with the rising influence of gas-phase

330

331

332

333

334

335

336

337

338

339

340

341

342

343

344

345

346

347

348

349

350

351

352

353

\*OH as LWC decreases, with the relative importance of aqueous and gaseous reactions depending on the Henry's law constant of the phenol. Our simple calculations suggest that for phenols with low to moderate  $K_{\rm H}$  values, gas-phase oxidation dominates across all LWC values at a fairly constant rate. In contrast, for phenols with high  $K_{\rm H}$  (above approximately  $10^7$  M atm<sup>-1</sup>), aqueous-phase reactions generally dominate SOA formation and the rate is sensitive to LWC. Overall, our calculations indicate that reactions of phenols with high  $K_{\rm H}$  values can be important pathways of SOA formation in aerosol liquid water, with this chemistry largely driven by  $^3$ C\* and  $^1$ O<sub>2</sub>\*.

# **FIGURES**

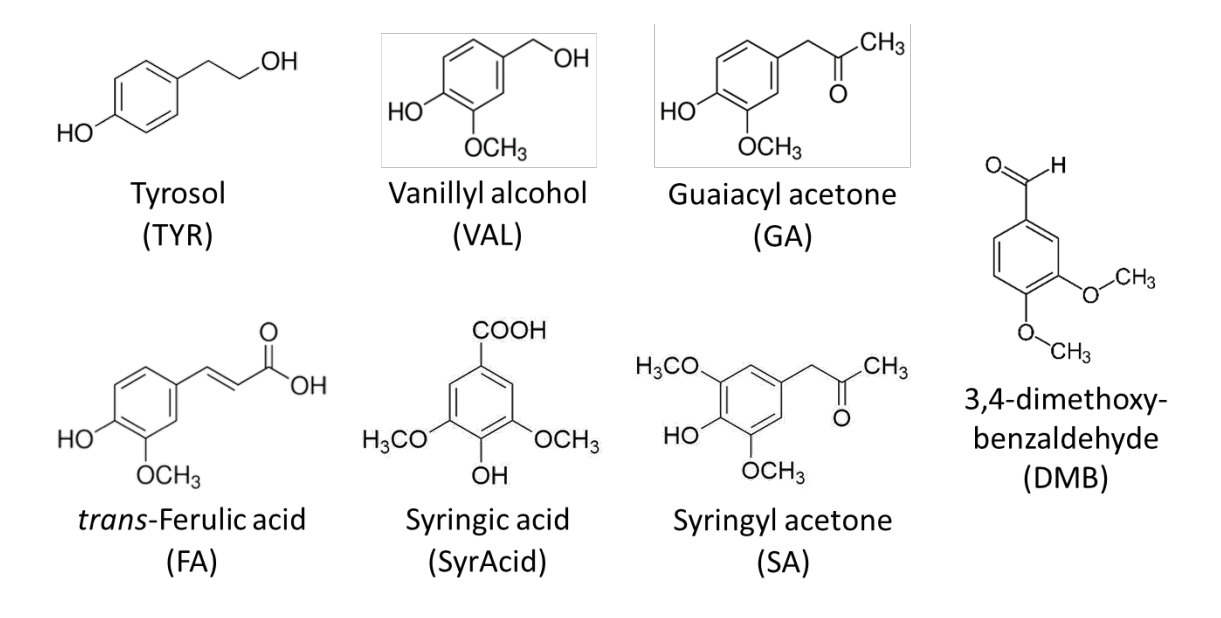


**Figure 1.** Chemical structures of phenols used in this study. The structure of the triplet precursor DMB is also shown.

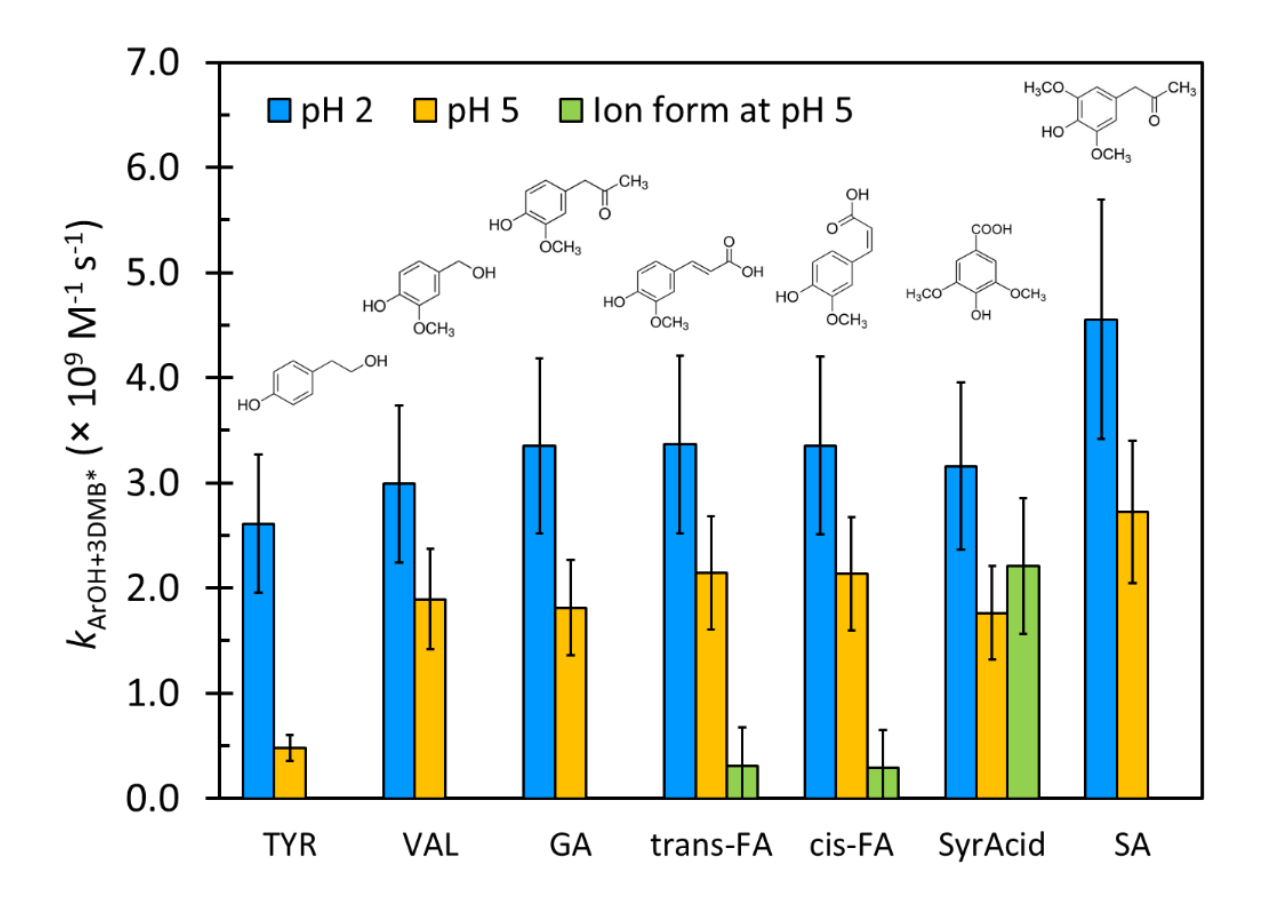


**Figure 2.** Second-order rate constants for phenols reacting with  $^3DMB^*$  at pH 2 and 5. The carboxylic acid groups in FA and SyrAcid (pK<sub>a</sub> = 4.6 and 4.2, respectively) are partially deprotonated at pH 5: the yellow bars represent kinetics for the neutral form while the green bars are for the carboxylate form. Error bars represent  $\pm$  1 standard error propagated from linear regression. Data are listed in Table S4.

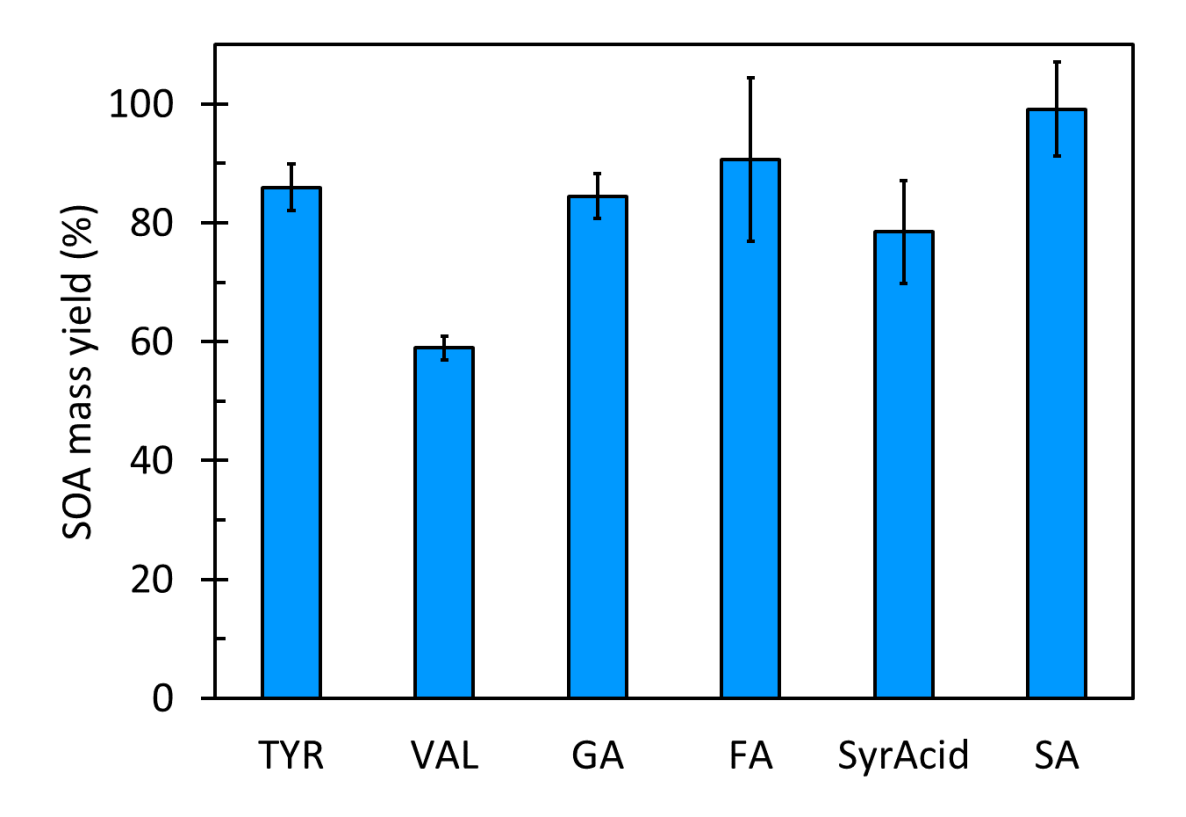


**Figure 3.** Aqueous SOA mass yields ( $Y_{SOA}$ ) from phenol oxidized by the DMB triplet state at pH 5. Error bars are  $\pm$  1 standard deviation, calculated from replicate samples at different times during the reaction, from one to three half-lives. The SA yield is statistically higher (p < 0.05) that those of the other compounds except for FA, while the VAL yield is statistically lower than all other values.

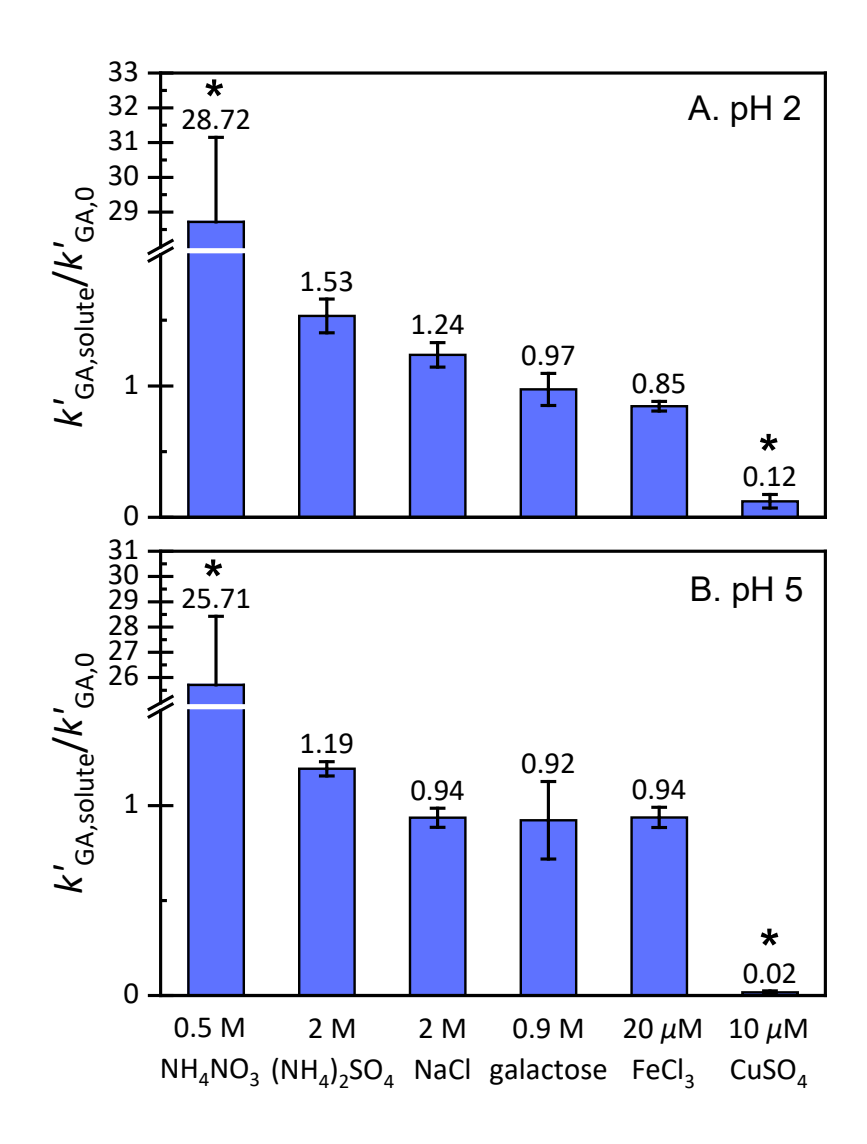


**Figure 4.** Effect of different solutes on the first-order rate constant of GA decay ( $k'_{GA}$ ) at pH 2 (panel A) and pH 5 (panel B): values are shown as the ratio of the GA loss rate constant with solute to the rate constant without solute, with both experiments performed on the same day. Solutions contained 10  $\mu$ M DMB, 10  $\mu$ M GA, H<sub>2</sub>SO<sub>4</sub> to adjust the pH, and the listed concentration of solute. Error bars represent  $\pm$  1 standard deviation. Asterisks represent a ratio that is statistically different from unity (p <0.05). For solutions containing FeCl<sub>3</sub>, we removed the portion of GA loss due to Fe chemistry to examine whether iron alters DMB-phenol kinetics; see Figure S9 for details.

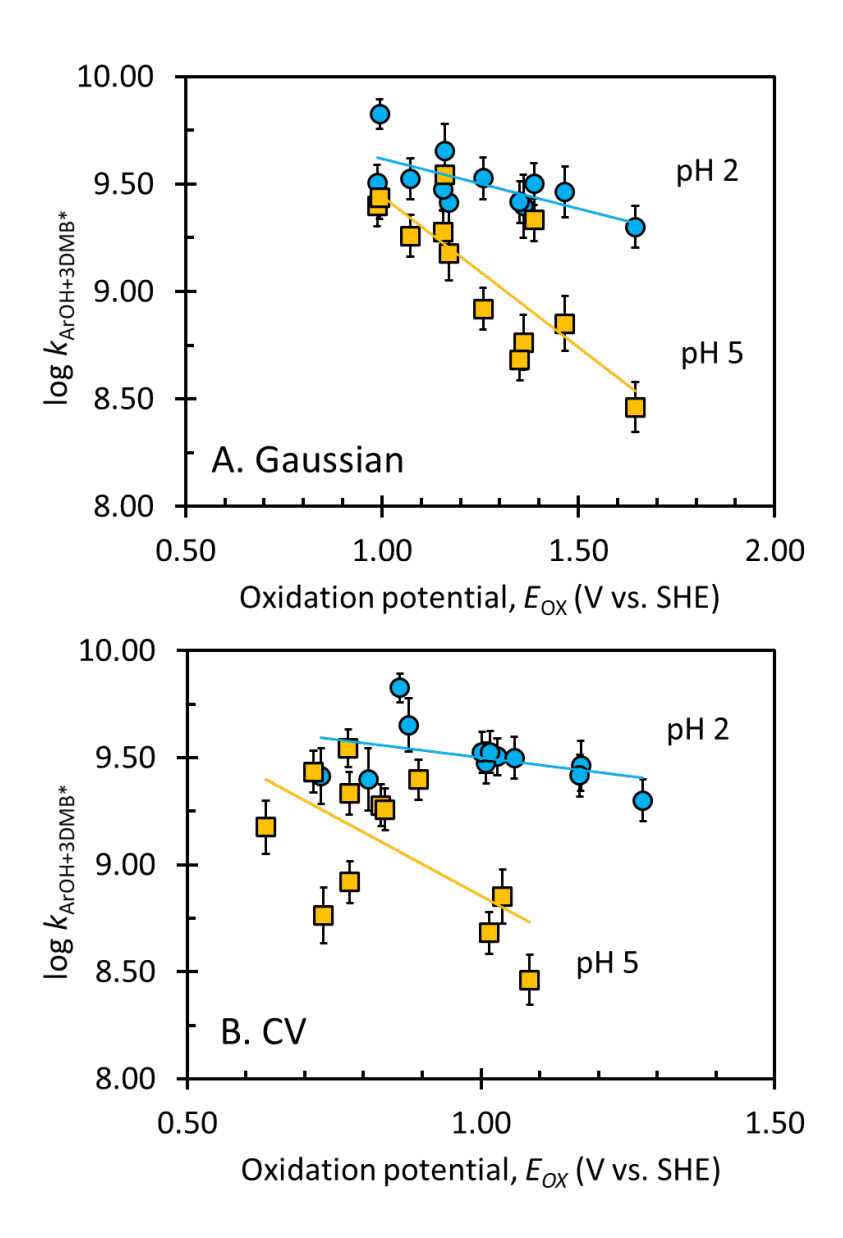


**Figure 5.** Correlation between measured bimolecular rate constants for phenols with the DMB triplet state and computed or measured one-electron oxidation potentials of phenols. Panel A shows QSARs based on oxidation potentials calculated by Gaussian:  $\log(k_{\text{ArOH+3DMB*}}) = -0.46E_{\text{OX}} + 10.1 \ (r^2 = 0.47) \ \text{at pH}$  2 and  $\log(k_{\text{ArOH+3DMB*}}) = -1.41E_{\text{OX}} + 10.8 \ (r^2 = 0.66) \ \text{at pH}$  5. Panel B shows QSARs based on oxidation potentials measured by cyclic voltammetry:  $\log(k_{\text{ArOH+3DMB*}}) = -0.34E_{\text{OX}} + 9.84 \ (r^2 = 0.16) \ \text{at pH}$  2 and  $\log(k_{\text{ArOH+3DMB*}}) = -1.48E_{\text{OX}} + 10.3 \ (r^2 = 0.36) \ \text{at pH}$  5). Error bars are  $\pm 1$  standard error of  $k_{\text{ArOH+3DMB*}}$ .

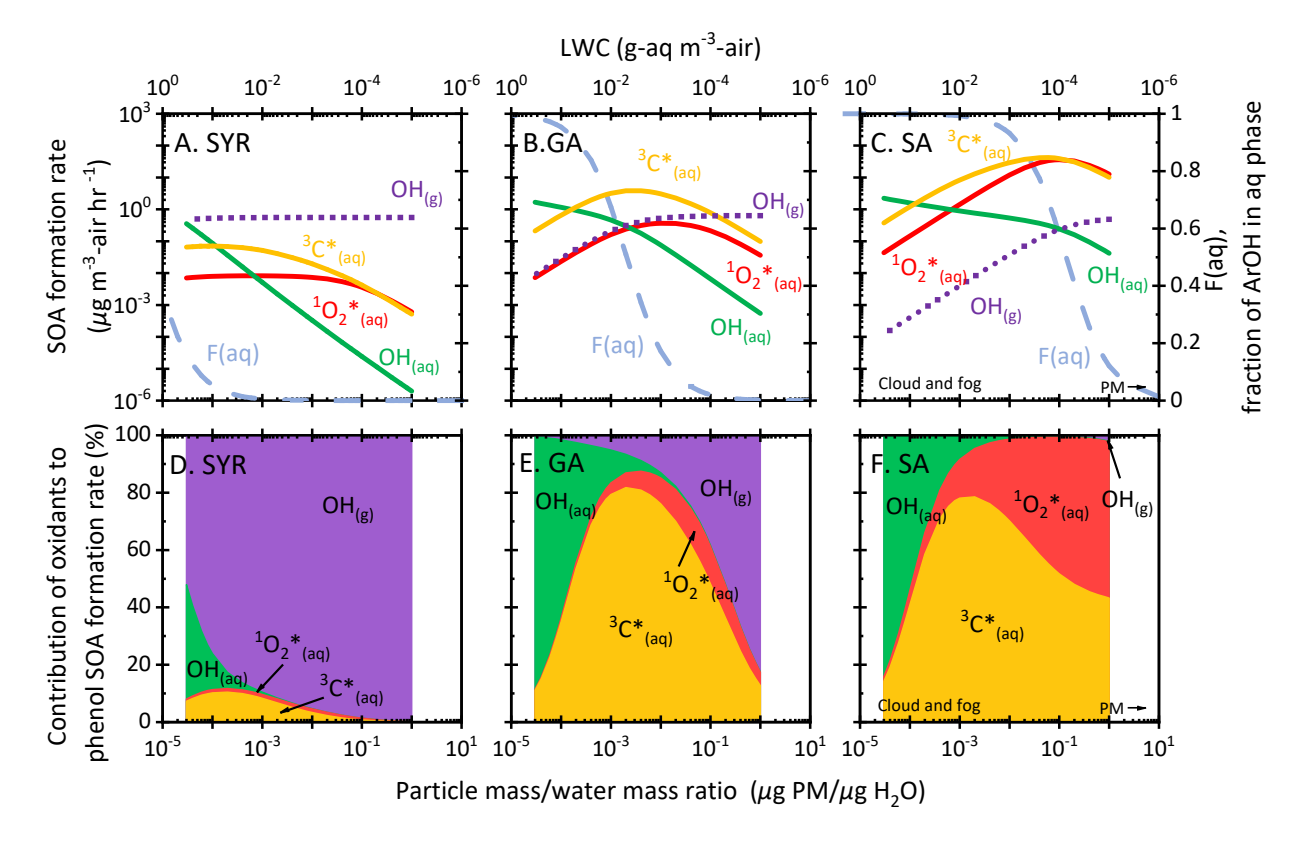


**Figure 6.** The top row (panels A-C) shows initial SOA formation rates from gas and aqueous reactions of syringol ( $K_{\rm H} = 2.5 \times 10^4 \,\mathrm{M}$  atm<sup>-1</sup> at 278 K), guaiacyl acetone ( $K_{\rm H} = 9.1 \times 10^6 \,\mathrm{M}$  atm<sup>-1</sup>), and syringyl acetone ( $K_{\rm H} = 6.1 \times 10^8 \,\mathrm{M}$  atm<sup>-1</sup>) as a function of liquid water content (top axis; assuming a PM concentration of  $10 \,\mu\mathrm{g}$  m<sup>-3</sup>) and particle mass/water mass ratio (bottom axis). The dotted line is the rate of SOA formation from gas-phase •OH with each phenol, while solid lines represent aqSOA formation rates for a given phenol with  ${}^3\mathrm{C}^*$ ,  ${}^1\mathrm{O}_2^*$ , and  ${}^4\mathrm{OH}$ ; see SI Section S6 for calculations. Aqueous oxidant concentrations vary with LWC: [ ${}^4\mathrm{OH}$ ] =  $(0.8 - 5) \times 10^{-15} \,\mathrm{M}^{-1}\mathrm{s}^{-1}$ , [ ${}^3\mathrm{C}^*$ ] =  $(0.008 - 2) \times 10^{-12} \,\mathrm{M}^{-1}\mathrm{s}^{-1}$ , [ ${}^1\mathrm{O}_2^*$ ] =  $(0.0007 - 1) \times 10^{-10} \,\mathrm{M}^{-1}\mathrm{s}^{-1}$ . The blue dashed line is the fraction of phenol in the aqueous phase, F(aq). The bottom row (panels D-F) shows the corresponding contribution of each oxidant to SOA formation from that phenol.

### **Supporting Information**

Direct photodegradation of phenols; methods for aqSOA mass yields determination; methods for phenol oxidation potential measurements and calculations; additional kinetic figures of phenol degradation by <sup>3</sup>DMB\*; photoisomerization of ferulic acid; tabulated 2<sup>nd</sup>-order rate constants of phenols with <sup>3</sup>DMB\*; 416 determination of  $k_{ArOH+3DMB}$ \* for the neutral and ion forms of FA and SyrAcid; time series of SOA mass yields; additional figures about solute effects; tabulated values of phenol oxidation potentials; calculation of SOA formation rates from syringol, GA, and SA; and determination of <sup>3</sup>DMB\* intersystem crossing 418 quantum yield. This information is available free of charge via the Internet at http://pubs.acs.org.

420

421

419

412

413

414

415

417

#### ACKNOWLEDGMENTS

- 422 This work was funded by National Science Foundation grant (AGS-1649212), the California Agricultural
- 423 Experiment Station (Projects CA-D-LAW-6403-RR and CA-D-ETX-2102-H), and a Jastro Shields
- 424 Research Award and Donald G. Crosby Fellowship from UC Davis to L.M.

425

426

#### REFERENCES

- 427 (1) Sommers, W. T.; Loehman, R. A.; Hardy, C. C. Wildland fire emissions, carbon, and climate: 428 science overview and knowledge needs. For. Ecol. Manag. 2014, 317, 1–8.
- 429 (2) Pöschl, U. Atmospheric aerosols: composition, transformation, climate and health effects. Angew. Chem. Int. Ed. Engl. 2005, 44, 7520-7540. 430
- Hallquist, M.; Wenger, J. C.; Baltensperger, U.; Rudich, Y.; Simpson, D.; Claeys, M.; Dommen, 431 (3)
- 432 J.; Donahue, N. M.; George, C.; Goldstein, A. H.; Hamilton, J. F.; Herrmann, H.; Hoffmann, T.;
- 433 Iinuma, Y.; Jang, M.; Jenkin, M. E.; Jimenez, J. L.; Kiendler-Scharr, A.; Maenhaut, W.;
- McFiggans, G.; Mentel, Th. F.; Monod, A.; Prévôt, A. S. H.; Seinfeld, J. H.; Surratt, J. D.; 434
- Szmigielski, R.; Wildt. J. The formation, properties and impact of secondary organic aerosol: 435
- current and emerging issues. Atmos. Chem. Phys. 2009, 9, 5155–5236. 436
- 437 Ervens, B.; Turpin, B. J.; Weber, R. J. Secondary organic aerosol formation in cloud droplets and 438 aqueous particles (aqSOA): a review of laboratory, field and model studies. Atmos. Chem. Phys.
- 439 **2011**, *11*, 11069–11102.

- 440 (5) McNeill, V. F. Aqueous organic chemistry in the atmosphere: sources and chemical processing of organic aerosols. *Environ. Sci. Technol.* **2015**, *49*, 1237–1244.
- Herrmann, H.; Schaefer, T.; Tilgner, A.; Styler, S. A.; Weller, C.; Teich, M.; Otto, T.

  Tropospheric aqueous-phase chemistry: kinetics, mechanisms, and its coupling to a changing gas phase. *Chem. Rev.* **2015**, *115*, 4259–4334.
- 445 (7) Bond, T. C.; Streets, D. G.; Yarber, K. F.; Nelson, S. M.; Woo, J.; Klimont, Z. A technology based global inventory of black and organic carbon emissions from combustion. *J. Geophys. Res.*447 *Atmos.* **2004**, *109*.
- 448 (8) Bruns, E. A.; El Haddad, I.; Slowik, J. G.; Kilic, D.; Klein, F.; Baltensperger, U.; Prévôt, A. S. H. Identification of significant precursor gases of secondary organic aerosols from residential wood combustion. *Sci. Rep.* **2016**, *6*, 27881.
- 451 (9) Oros, D. R.; Simoneit, B. R. Identification and emission factors of molecular tracers in organic aerosols from biomass burning Part 1. Temperate climate conifers. *Applied Geochemistry* **2001**, 16, 1513–1544.
- 454 (10) Schauer, J. J.; Kleeman, M. J.; Cass, G. R.; Simoneit, B. R. Measurement of emissions from air pollution sources. 3. C1-C29 organic compounds from fireplace combustion of wood. *Environ.* 456 *Sci. Technol.* **2001**, *35*, 1716–1728.
- 457 (11) Simoneit, B. R. Biomass burning a review of organic tracers for smoke from incomplete combustion. *Applied Geochemistry* **2002**, *17*, 129–162.
- 459 (12) Andreae, M. O. Emission of trace gases and aerosols from biomass burning an updated assessment. *Atmos. Chem. Phys.* **2019**, *19*, 8523–8546.
- 461 (13) Sagebiel, J. C.; Seiber, J. N.; Woodrow, J. E. Comparison of headspace and gas-stripping methods 462 for determining the Henry's law constant (H) for organic compounds of low to intermediate H. 463 *Chemosphere* **1992**, *25*, 1763–1768.
- 464 (14) Feigenbrugel, V.; Le Calvé, S.; Mirabel, P.; Louis, F. Henry's law constant measurements for phenol, o-, m-, and p-cresol as a function of temperature. *Atmospheric Environment* **2004**, *38*, 5577–5588.
- 467 (15) McFall, A. S.; Johnson, A. W.; Anastasio, C. Air-Water Partitioning of Biomass-Burning Phenols and the Effects of Temperature and Salinity. *Environ. Sci. Technol.* **2020**, *54*, 3823–3830.
- 469 (16) Smith, J. D.; Kinney, H.; Anastasio, C. Aqueous benzene-diols react with an organic triplet 470 excited state and hydroxyl radical to form secondary organic aerosol. *Phys. Chem. Chem. Phys.* 471 **2015**, *17*, 10227–10237.
- 472 (17) Sun, Y. L.; Zhang, Q.; Anastasio, C.; Sun, J. Insights into secondary organic aerosol formed via 473 aqueous-phase reactions of phenolic compounds based on high resolution mass spectrometry. 474 *Atmos. Chem. Phys.* **2010**, *10*, 4809–4822.
- Vione, D.; Maurino, V.; Minero, C.; Duncianu, M.; Olariu, R.-I.; Arsene, C.; Sarakha, M.;
   Mailhot, G. Assessing the transformation kinetics of 2-and 4-nitrophenol in the atmospheric aqueous phase. Implications for the distribution of both nitroisomers in the atmosphere.
   Atmospheric Environment 2009, 43, 2321–2327.

- 479 (19) Smith, J. D.; Sio, V.; Yu, L.; Zhang, Q.; Anastasio, C. Secondary organic aerosol production from aqueous reactions of atmospheric phenols with an organic triplet excited state. *Environ. Sci.*481 *Technol.* **2014**, *48*, 1049–1057.
- 482 (20) Anastasio, C.; Faust, B. C.; Rao, C. J. Aromatic carbonyl compounds as aqueous-phase 483 photochemical sources of hydrogen peroxide in acidic sulfate aerosols, fogs, and clouds. 1. Non-484 phenolic methoxybenzaldehydes and methoxyacetophenones with reductants (phenols). *Environ.* 485 *Sci. Technol.* **1996**, *31*, 218–232.
- 486 (21) Rossignol, S.; Aregahegn, K. Z.; Tinel, L.; Fine, L.; Nozière, B.; George, C. Glyoxal induced 487 atmospheric photosensitized chemistry leading to organic aerosol growth. *Environ. Sci. Technol.* 488 **2014**, 48, 3218–3227.
- 489 (22) Aregahegn, K. Z.; Nozière, B.; George, C. Organic aerosol formation photo-enhanced by the formation of secondary photosensitizers in aerosols. *Faraday Discuss* **2013**, *165*, 123–134.
- 491 (23) Mekic, M.; Liu, J.; Zhou, W.; Loisel, G.; Cai, J.; He, T.; Jiang, B.; Yu, Z.; Lazarou, Y. G.; Li, X.;
   492 Brigante, M.; Vione, D.; Gligorovski, S. Formation of highly oxygenated multifunctional
   493 compounds from cross-reactions of carbonyl compounds in the atmospheric aqueous phase.
   494 Atmos. Environ. 2019, 219, 117046.
- 495 (24) Xia, S.-S.; Eugene, A. J.; Guzman, M. I. Cross photoreaction of glyoxylic and pyruvic acids in model aqueous aerosol. *J. Phys. Chem. A* **2018**, *122*, 6457–6466.
- 497 (25) Wang, X.; Gemayel, R.; Hayeck, N.; Perrier, S.; Charbonnel, N.; Xu, C.; Chen, H.; Zhu, C.;
  498 Zhang, L.; Wang, L.; Nizkorodov, S. A.; Wang, X.; Wang, Z.; Wang, T.; Mellouki, A.; Riva, M.;
  499 Chen, J.; George C. Atmospheric photosensitization: A new pathway for sulfate formation.
  500 Environ. Sci. Technol. 2020, 54, 3114–3120.
- 501 (26) Herrmann, H.; Hoffmann, D.; Schaefer, T.; Bräuer, P.; Tilgner, A. Tropospheric aqueous-phase 502 free-radical chemistry: radical sources, spectra, reaction kinetics and prediction tools. 503 *ChemPhysChem* **2010**, *11*, 3796–3822.
- 504 (27) Kaur, R.; Anastasio, C. First measurements of organic triplet excited states in atmospheric waters. 505 *Environ. Sci. Technol.* **2018**, *52*, 5218–5226.
- Kaur, R.; Labins, J. R.; Helbock, S. S.; Jiang, W.; Bein, K. J.; Zhang, Q.; Anastasio, C.
   Photooxidants from brown carbon and other chromophores in illuminated particle extracts. *Atmos. Chem. Phys.* 2019, 19, 6579–6594.
- 509 (29) Buxton, G. V.; Greenstock, C. L.; Helman, W. P.; Ross, A. B. Critical Review of rate constants 510 for reactions of hydrated electrons, hydrogen atoms and hydroxyl radicals (•OH/•O<sup>-</sup> in Aqueous 511 Solution. *J. Phys. Chem. Ref. Data* **1988**, *17*, 513–886.
- 512 (30) Yu, L.; Smith, J.; Laskin, A.; Anastasio, C.; Laskin, J.; Zhang, Q. Chemical characterization of SOA formed from aqueous-phase reactions of phenols with the triplet excited state of carbonyl and hydroxyl radical. *Atmos. Chem. Phys.* **2014**, *14*, 13801–13816.
- 515 (31) Herrmann, H. Kinetics of aqueous phase reactions relevant for atmospheric chemistry. *Chem. Rev.* **2003**, *103*, 4691–4716.

- Volkamer, R.; San Martini, F.; Molina, L. T.; Salcedo, D.; Jimenez, J. L.; Molina, M. J. A missing sink for gas-phase glyoxal in Mexico City: Formation of secondary organic aerosol. *Geophys*.
- 519 Res. Lett. **2007**, 34.
- 520 (33) Faust, J. A.; Wong, J. P. S.; Lee, A. K. Y.; Abbatt, J. P. D. Role of Aerosol Liquid Water in 521 Secondary Organic Aerosol Formation from Volatile Organic Compounds. *Environ. Sci. Technol.*
- **2017**, *51*, 1405–1413.
- Nguyen, T. K. V.; Zhang, Q.; Jimenez, J. L.; Pike, M.; Carlton, A. G. Liquid water: ubiquitous contributor to aerosol mass. *Environ. Sci. Technol. Lett.* **2016**, *3*, 257–263.
- 525 (35) Seinfeld, J. H.; Pandis, S. N. *Atmospheric Chemistry And Physics: From Air Pollution To Climate Change*; 3rd ed.; Wiley: Hoboken, New Jersey, 2016; p. 1152.
- 527 (36) Mekic, M.; Brigante, M.; Vione, D.; Gligorovski, S. Exploring the ionic strength effects on the 528 photochemical degradation of pyruvic acid in atmospheric deliquescent aerosol particles. *Atmos.* 529 *Environ.* **2018**, *185*, 237–242.
- Zhou, W.; Mekic, M.; Liu, J.; Loisel, G.; Jin, B.; Vione, D.; Gligorovski, S. Ionic strength effects
   on the photochemical degradation of acetosyringone in atmospheric deliquescent aerosol particles.
   Atmos. Environ. 2019, 198, 83–88.
- 533 (38) Parworth, C. L.; Young, D. E.; Kim, H.; Zhang, X.; Cappa, C. D.; Collier, S.; Zhang, Q.
  534 Wintertime water-soluble aerosol composition and particle water content in Fresno, California. *J. Geophys. Res. Atmos.* **2017**, *122*, 3155–3170.
- 536 (39) Oros, D. R.; Simoneit, B. R. Identification and emission factors of molecular tracers in organic 537 aerosols from biomass burning Part 2. Deciduous trees. *Applied Geochemistry* **2001**, *16*, 1545– 538 1565.
- 539 (40) Zangrando, R.; Barbaro, E.; Zennaro, P.; Rossi, S.; Kehrwald, N. M.; Gabrieli, J.; Barbante, C.;
   540 Gambaro, A. Molecular markers of biomass burning in Arctic aerosols. *Environ. Sci. Technol.* 541 2013, 47, 8565–8574.
- Hoffmann, D.; Iinuma, Y.; Herrmann, H. Development of a method for fast analysis of phenolic molecular markers in biomass burning particles using high performance liquid chromatography/atmospheric pressure chemical ionisation mass spectrometry. *J. Chromatogr. A* **2007**, *1143*, 168–175.
- 546 (42) Fleming, L. T.; Lin, P.; Roberts, J. M.; Selimovic, V.; Yokelson, R.; Laskin, J.; Laskin, A.;
   547 Nizkorodov, S. A. Molecular composition and photochemical lifetimes of brown carbon
   548 chromophores in biomass burning organic aerosol. *Atmos. Chem. Phys.* 2020, 20, 1105–1129.
- 549 (43) Anastasio, C.; McGregor, K. G. Chemistry of fog waters in California's Central Valley: 1. In situ photoformation of hydroxyl radical and singlet molecular oxygen. *Atmos. Environ.* **2001**, *35*, 551 1079–1089.
- Jiang, W.; Misovich, M. H.; Anusha Priyadarshani Silva; McFall, A.; Anastasio, C.; Zhang, Q.
   Photosensitized Reactions of a Phenolic Carbonyl from Wood Combustion in the Aqueous Phase
   Chemical Evolution and Light Absorption Properties of AqSOA. *Environ. Sci. Technol.* 2021
   (in press).

- Canonica, S.; Hoigné, J. Enhanced oxidation of methoxy phenols at micromolar concentration photosensitized by dissolved natural organic material. *Chemosphere* **1995**, *30*, 2365–2374.
- Ragnar, M.; Lindgren, C. T.; Nilvebrant, N. O. pK<sub>a</sub> -Values of Guaiacyl and Syringyl Phenols Related to Lignin. *Journal of Wood Chemistry and Technology* **2000**, *20*, 277–305.
- 560 (47) Erdemgil, F. Z.; Şanli, S.; Şanli, N.; Özkan, G.; Barbosa, J.; Guiteras, J.; Beltran, J. L.
   561 Determination of pKa values of some hydroxylated benzoic acids in methanol—water binary
   562 mixtures by LC methodology and potentiometry. *Talanta* 2007, 72, 489–496.
- 563 (48) Canonica, S.; Hellrung, B.; Wirz, J. Oxidation of phenols by triplet aromatic ketones in aqueous solution. *The Journal of Physical Chemistry A* **2000**, *104*, 1226–1232.
- Jonsson, M.; Lind, J.; Reitberger, T.; Eriksen, T. E.; Merenyi, G. Free radical combination reactions involving phenoxyl radicals. *The Journal of Physical Chemistry* **1993**, *97*, 8229–8233.
- 567 (50) Grebel, J. E.; Pignatello, J. J.; Mitch, W. A. Sorbic acid as a quantitative probe for the formation, 568 scavenging and steady-state concentrations of the triplet-excited state of organic compounds. 569 *Water Res.* **2011**, *45*, 6535–6544.
- 570 (51) Schmitt, M.; Moor, K. J.; Erickson, P. R.; McNeill, K. Sorbic acid as a triplet probe: reactivity of oxidizing triplets in dissolved organic matter by direct observation of aromatic amine oxidation.

  572 Environ. Sci. Technol. 2019, 53, 8087–8096.
- Yee, L. D.; Kautzman, K. E.; Loza, C. L.; Schilling, K. A.; Coggon, M. M.; Chhabra, P. S.; Chan,
   M. N.; Chan, A. W. H.; Hersey, S. P.; Crounse, J. D.; Wennberg, P. O.; Flagan, R. C.; Seinfeld, J.
   H. Secondary organic aerosol formation from biomass burning intermediates: phenol and
   methoxyphenols. *Atmos. Chem. Phys.* 2013, 13, 8019–8043.
- 577 (53) Lauraguais, A.; Coeur-Tourneur, C.; Cassez, A.; Seydi, A. Rate constant and secondary organic 578 aerosol yields for the gas-phase reaction of hydroxyl radicals with syringol (2, 6-579 dimethoxyphenol). *Atmos. Environ.* **2012**, *55*, 43–48.
- 580 (54) Tang, I. N.; Munkelwitz, H. R. Water activities, densities, and refractive indices of aqueous 581 sulfates and sodium nitrate droplets of atmospheric importance. *J. Geophys. Res. Atmos.* **1994**, *99*, 582 18801–18808.
- 583 (55) Sareen, N.; Schwier, A. N.; Shapiro, E. L.; Mitroo, D.; McNeill, V. F. Secondary organic material formed by methylglyoxal in aqueous aerosol mimics. *Atmos. Chem. Phys.* **2010**, *10*, 997–1016.
- Parker, K. M.; Pignatello, J. J.; Mitch, W. A. Influence of ionic strength on triplet-state natural organic matter loss by energy transfer and electron transfer pathways. *Environ. Sci. Technol.* **2013**, *47*, 10987–10994.
- 588 (57) Grebel, J. E.; Pignatello, J. J.; Mitch, W. A. Impact of halide ions on natural organic matter 589 sensitized photolysis of 17β-estradiol in saline waters. *Environ. Sci. Technol.* 2012, 46, 7128–
   590 7134.
- 591 (58) Simoneit, B. R.; Schauer, J. J.; Nolte, C. G.; Oros, D. R.; Elias, V. O.; Fraser, M. P.; Rogge, W.
   592 F.; Cass, G. R. Levoglucosan, a tracer for cellulose in biomass burning and atmospheric particles.
   593 Atmospheric Environment 1999, 33, 173–182.

- 594 (59) Mao, J.; Fan, S.; Jacob, D. J.; Travis, K. R. Radical loss in the atmosphere from Cu-Fe redox coupling in aerosols. *Atmos. Chem. Phys.* **2013**, *13*, 509–519.
- 596 (60) Deguillaume, L.; Leriche, M.; Desboeufs, K.; Mailhot, G.; George, C.; Chaumerliac, N.
  597 Transition metals in atmospheric liquid phases: sources, reactivity, and sensitive parameters.
  598 *Chem. Rev.* **2005**, *105*, 3388–3431.
- 599 (61) Brezonik, P. L.; Fulkerson-Brekken, J. Nitrate-Induced Photolysis in Natural Waters: Controls on
   600 Concentrations of Hydroxyl Radical Photo-Intermediates by Natural Scavenging Agents. *Environ.* 601 Sci. Technol. 1998, 32, 3004–3010.
- 602 (62) Chu, L.; Anastasio, C. Quantum Yields of Hydroxyl Radical and Nitrogen Dioxide from the Photolysis of Nitrate on Ice. *J. Phys. Chem. A* **2003**, *107*, 9594–9602.
- 604 (63) Ming, G.; Zhenhao, D. Prediction of oxygen solubility in pure water and brines up to high temperatures and pressures. *Geochim. Cosmochim. Acta* **2010**, *74*, 5631–5640.
- 606 (64) Millero, F. J.; Huang, F.; Laferiere, A. L. The solubility of oxygen in the major sea salts and their mixtures at 25 C. *Geochim. Cosmochim. Acta* **2002**, *66*, 2349–2359.
- 608 (65) Feng, W.; Nansheng, D. Photochemistry of hydrolytic iron (III) species and photoinduced degradation of organic compounds. A minireview. *Chemosphere* **2000**, *41*, 1137–1147.
- 610 (66) Pang, H.; Zhang, Q.; Wang, H.; Cai, D.; Ma, Y.; Li, L.; Li, K.; Lu, X.; Chen, H.; Yang, X.; Chen, Gl1 J. Photochemical Aging of Guaiacol by Fe(III)-Oxalate Complexes in Atmospheric Aqueous Phase. *Environ. Sci. Technol.* **2019**, *53*, 127–136.
- Khanra, S.; Minero, C.; Maurino, V.; Pelizzetti, E.; Dutta, B. K.; Vione, D. Phenol transformation induced by UVA photolysis of the complex FeCl2+. *Environ Chem Lett* **2008**, *6*, 29–34.
- 615 (68) Pan, Y.; Garg, S.; Waite, T. D.; Yang, X. Copper Inhibition of Triplet-Induced Reactions 616 Involving Natural Organic Matter. *Environ. Sci. Technol.* **2018**, *52*, 2742–2750.
- 617 (69) Pan, Y.; Ruan, X.; Garg, S.; Waite, T. D.; Lei, Y.; Yang, X. Copper Inhibition of Triplet-618 Sensitized Phototransformation of Phenolic and Amine Contaminants. *Environ. Sci. Technol.* 619 **2020**, *54*, 9980–9989.
- 620 (70) Buerge-Weirich, D.; Sulzberger, B. Formation of Cu(I) in Estuarine and Marine 621 Waters: Application of a New Solid-Phase Extraction Method To Measure Cu(I). *Environ. Sci.* 622 *Technol.* **2004**, *38*, 1843–1848.
- 623 (71) Bielski, B. H. J.; Cabelli, D. E.; Arudi, R. L.; Ross, A. B. Reactivity of HO<sub>2</sub> /O<sub>2</sub><sup>-</sup> radicals in aqueous solution. *J. Phys. Chem. Ref. Data* **1985**, *14*, 1041–1100.
- 625 (72) Rabani, J.; Klug-Roth, D.; Lilie, J. Pulse radiolytic investigations of the catalyzed 626 disproportionation of peroxy radicals. Aqueous cupric ions. *J. Phys. Chem.* **1973**, 77, 1169–1175.
- 627 (73) Chan, L. K.; Nguyen, K. Q.; Karim, N.; Yang, Y.; Rice, R. H.; He, G.; Denison, M. S.; Nguyen, 628 T. B. Relationship between the molecular composition, visible light absorption, and health-related 629 properties of smoldering woodsmoke aerosols. *Atmos. Chem. Phys.* **2020**, *20*, 539–559.
- Kaur, R.; Hudson, B. M.; Draper, J.; Tantillo, D. J.; Anastasio, C. Aqueous reactions of organic triplet excited states' with atmospheric alkenes. *Atmos. Chem. Phys.* **2019**, *19*, 5021–5032.

- 632 (75) Arnold, W. A. One electron oxidation potential as a predictor of rate constants of N-containing compounds with carbonate radical and triplet excited state organic matter. *Environ. Sci. Process.* 634 *Impacts* **2014**, *16*, 832–838.
- 635 (76) Arnold, W. A.; Oueis, Y.; O'Connor, M.; Rinaman, J. E.; Taggart, M. G.; McCarthy, R. E.;
  636 Foster, K. A.; Latch, D. E. QSARs for phenols and phenolates: oxidation potential as a predictor
  637 of reaction rate constants with photochemically produced oxidants. *Environmental Science:*638 *Processes & Impacts* **2017**, *19*, 324–338.
- 639 (77) Suatoni, J. C.; Snyder, R. E.; Clark, R. O. Voltammetric studies of phenol and aniline ring substitution. *Anal. Chem.* **1961**, *33*, 1894–1897.
- 641 (78) Pavitt, A. S.; Bylaska, E. J.; Tratnyek, P. G. Oxidation potentials of phenols and anilines: 642 correlation analysis of electrochemical and theoretical values. *Environ. Sci. Process. Impacts* 643 **2017**, *19*, 339–349.
- 644 (79) Li, C.; Hoffman, M. Z. One-Electron Redox Potentials of Phenols in Aqueous Solution. *J. Phys. Chem. B* **1999**, *103*, 6653–6656.
- Winget, P.; Cramer, C. J.; Truhlar, D. G. Computation of equilibrium oxidation and reduction
   potentials for reversible and dissociative electron-transfer reactions in solution. *Theor. Chem. Acc.* 2004, 112(4), 217–227.

1	Supporting Information for		
2	Kinetics and Mass Yields of Aqueous Secondary Organic		
3	Aerosol from Highly Substituted Phenols Reacting with a		
4	Triplet Excited State		
5	Lan Ma <sup>1</sup> , Chrystal Guzman <sup>1</sup> , Christopher Niedek <sup>2</sup> , Theodore Tran <sup>1</sup> , Qi Zhang <sup>2</sup> , and Cort		
6	$Anastasio^{l}*$		
7	<sup>1</sup> Department of Land, Air, and Water Resource, University of California, Davis, CA 95616		
8	<sup>2</sup> Department of Environmental Toxicology, University of California, Davis, CA 95616		
9	Correspondence to: Cort Anastasio (canastasio@ucdavis.edu)		
10			
11			
12	This Supporting Information contains 27 pages and includes:		
13	7 texts, 11 figures, and 7 tables		
14			

**Table of Contents** 

- 17 **Section S1:** Direct photodegradation of phenols
- 18 **Section S2:** Phenolic aqSOA mass yields determination
- 19 **Section S3:** Determination of phenol oxidation potentials
- 20 **Section S4:** Photoisomerization of ferulic acid
- Section S5: Determination of  $k_{ArOH+3DMB}$ \* for neutral and ion (carboxylate) forms of FA and SyrAcid
- Section S6: Calculation of ambient SOA formation rates from syringol, guaiacyl acetone, and syringyl acetone
- 24 **Section S7:** Determination of intersystem crossing quantum yield
- Figure S1: Summary of the normalized first-order direct photodegradation rate constants for *trans*-FA, SA, and SyrAcid at different initial phenol concentrations at pH 2 and pH 5
- Figure S2: Representative plots of the aqueous oxidation of phenols by <sup>3</sup>DMB\* at pH 2 and pH 5
- Figure S3: Concentrations of *trans*-FA, *cis*-FA, and total FA as a result of photoisomerization
- Figure S4: Representative plot of *trans*-FA and *cis*-FA decay with illumination when reacting with 30 3DMB\* at pH 2 and pH 5
- Figure S5: Inverse of the phenol first-order decay rate constant as a function of the initial phenol concentrations at pH 2 and pH 5
- Figure S6: Time series of SOA yields at time zero and at one, two, and three phenol half-lives
- Figure S7: Dependence of the first-order rate constant of DMB decay on the concentration of ammonium nitrate
- Figure S8: Dependence of the first-order rate constant of GA decay on the concentration of solutes after correction for light screening
- Figure S9: Decay of GA by <sup>3</sup>DMB\* with presence of Fe(III)
- Figure S10: Comparison of measured oxidation potentials from cyclic voltammetry, computed values from Gaussian, and previous measures literature values
- Figure S11: Experimental results of the decay of SYR reacting with <sup>3</sup>DMB\* at 313 nm in experiments to determine the intersystem crossing quantum yield
- 43 **Table S1:** HPLC methods used to quantify ArOH concentrations
- Table S2: Measured or estimated values of parameters in Equation 2
- 45 **Table S3:** Regression parameters and coefficients derived from plots of 1/k'<sub>ArOH</sub> versus [ArOH]
- Table S4: Second-order rate constants of phenols with <sup>3</sup>DMB\* at pH 2 and 5
- Table S5: Oxidation potentials ( $E_{OX}$ ) measured by cyclic voltammetry (CV) and calculated using Gaussian 09
- Table S6: Gas- and aqueous-phase reaction rate constants and SOA mass yields of SYR, SA, and GA with the major oxidants
- Table S7: Summary of measured data for the quantum yield of <sup>3</sup>DMB\* intersystem crossing

**Table S1:** HPLC methods used to quantify ArOH concentrations. All methods had a flow rate of 0.6 mL min<sup>-1</sup>.

Compound	Compound Eluent <sup>a</sup>	
	(Vol:Vol)	wavelength
		(nm)
TYR	20%:80% ACN <sup>b</sup> : H <sub>2</sub> O	280
VAL	20%:80% ACN: H <sub>2</sub> O	280
GA	20%:80% ACN: H <sub>2</sub> O	280
FA	20%:80% ACN: 2% acetic acid in H <sub>2</sub> O	320
SyrAcid	20%:80% ACN: 2% acetic acid in $H_2O$	280
SA	15%:85% ACN: H <sub>2</sub> O	280

<sup>&</sup>lt;sup>a</sup> HPLC instrumentation: Shimadzu LC-10AT pump, ThermoScientific BetaBasic-18  $C_{18}$  column (250 × 3mm, 5  $\mu$ m bead), and Shimadzu-10AT UV-Vis detector

**Table S2:** Measured or estimated values of parameters in Equation 2. Uncertainties represent  $\pm 1$  standard error.

Parameters	Values	Reference	
Фіяс	0.095 (± 0.017)	This work (Section S7)	
<b>A</b> 12C		Smith et al. (2015)1	
Rate of <sup>3</sup> DMB* formation <sup>a</sup>	$4.9 (\pm 0.98)$	Smith <i>et al.</i> (2015) <sup>1</sup>	
$(j_{\text{hv,DMB}}\Phi_{\text{ISC}}[\text{DMB}], \mu\text{M min}^{-1})$	4.9 (± 0.98)	Silitii et al. (2013)	
$k_{\rm O2+3DMB^*}  ({ m M}^{-1}  { m s}^{-1})$	$2.8 (\pm 0.4) \times 10^9$	Kaur <i>et al.</i> $(2018)^2$	
$[\mathrm{O}_2]~(\mu\mathrm{M})^{\mathrm{b}}$	284	Rounds <i>et al.</i> (2006) <sup>3</sup>	

<sup>&</sup>lt;sup>a</sup> Rate of <sup>3</sup>DMB\* formation in a 10  $\mu$ M DMB solution illuminated with the equivalent of midday, winter solstice sunlight at Davis (i.e.  $j_{2NB} = 0.007 \text{ s}^{-1}$ ). The rate was calculated with the new value of  $\Phi_{ISC}$ .

<sup>&</sup>lt;sup>b</sup> ACN = acetonitrile

<sup>&</sup>lt;sup>b</sup> Value at 298 K

70 Some phenols with carbonyl or other chromophoric substituents absorb sunlight and undergo rapid direct 71 photodecay. 4.5 To test if this occurs for the phenols employed in this study over the time of our 72 experiments with  ${}^{3}DMB^{*}$ , we illuminated a solution containing 5-100  $\mu M$  of one phenol at pH 2 and 5 73 without addition of DMB, and measured the direct photodegradation rate constant ( $j_{ArOH}$ ). 74 We found no significant direct photodegradation of TYR, VAL, and GA, consistent with their very low 75 rates of sunlight absorption. However, FA, SA and SyrAcid do absorb sunlight significantly and undergo photodegradation; as described in the main text, we correct our triplet results for the direct photodecay of 76 77 these three phenols. Figure S1 shows their direct photodegradation rate constants as a function of initial 78 phenol concentrations. For FA, the rate constant of photodegradation doesn't change with FA 79 concentration (after correction for internal light screening) and has an average value of  $2.4 (\pm 0.6) \times 10^{-4}$ 80  $min^{-1}$  at pH 2 and 4.3 (± 1.1) ×  $10^{-4}$  min<sup>-1</sup> at pH 5. Based on these values, direct photodegradation of FA is 81 minor in our <sup>3</sup>DMB\* experiments, accounting for 6% or less of total FA decay in the presence of DMB. 82 For SyrAcid, photodegradation is initially very slow but then accelerates with illumination time, not 83 following first-order decay. These kinetics suggest SyrAcid photodecay forms compounds that initiate the 84 decay of SyrAcid via pathways other than direct photodecay (e.g. by producing an efficient photosensitizer). The  $j_{SyrAcid}$  values shown here are for the initial stage of the photodegradation. Rate 85 constants are independent of concentration, with average j values of  $0.36 (\pm 0.19) \times 10^{-3} \text{ min}^{-1}$  at pH 2 and 86  $2.7 (\pm 0.7) \times 10^{-3} \text{ min}^{-1}$  at pH 5. Over the illumination duration of our <sup>3</sup>DMB\* experiments, SyrAcid 87 88 photodegradation is slow at pH 2, contributing less than 5% of total SyrAcid decay in the illuminated 89 solution containing DMB. At pH 5, direct photodecay of SyrAcid accounts for about 15 to 30 % of decay 90 in the triplet experiments. In the case of SA, the photolysis rate constant generally increases with SA

69

91 92

93

94

95

in the presence of <sup>3</sup>DMB\*.

**Section S1:** Direct photodegradation of phenols

S4

concentration (Figure S1). At pH 2,  $j_{SA}$  ranges from  $2.0 \times 10^{-3}$  min<sup>-1</sup> to  $12.5 \times 10^{-3}$  min<sup>-1</sup> and from  $0.5 \times 10^{-3}$ 

min<sup>-1</sup> to 3.9 ×10<sup>-3</sup> min<sup>-1</sup> at pH 5. Direct photodecay of SA contributes 3%~34% of total SA loss measured

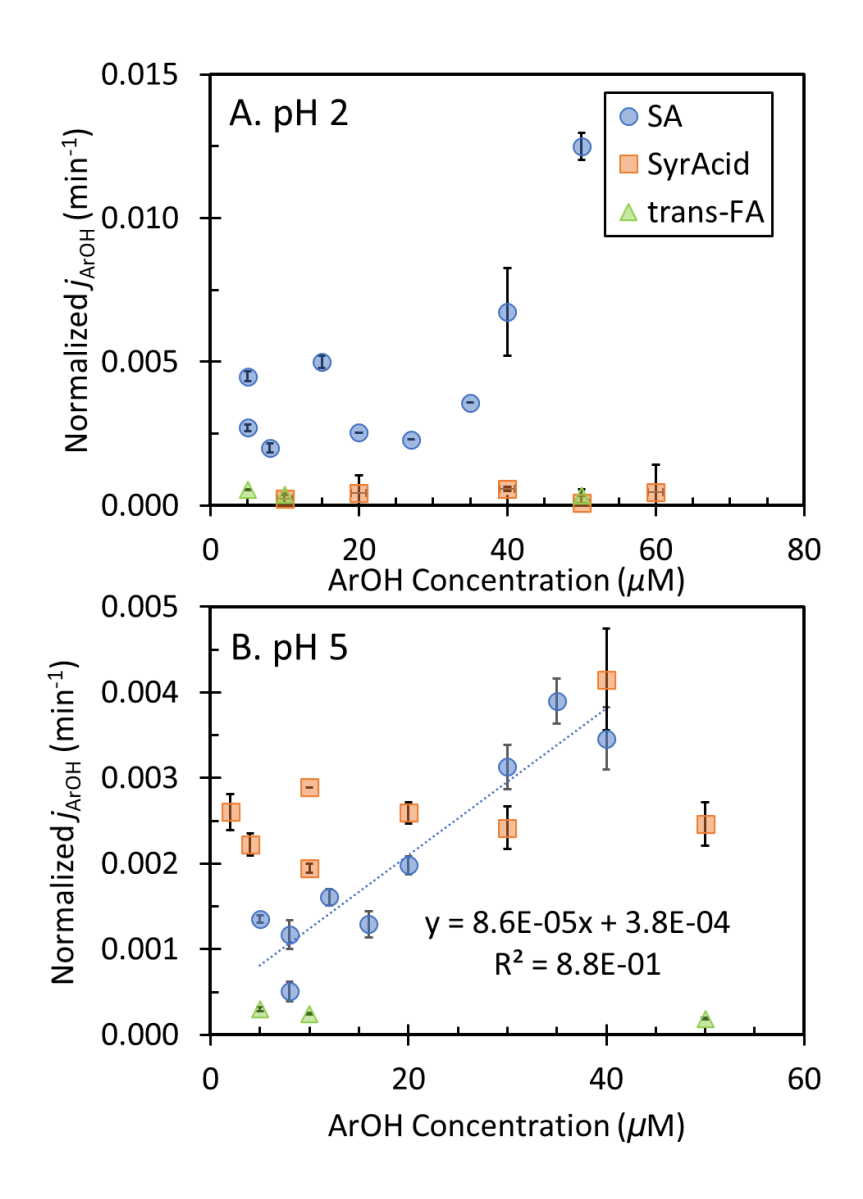


**Figure S1:** Summary of the normalized first-order direct photodegradation rate constants for *trans*-FA (green triangle), SA (blue circle), and SyrAcid (orange square) at different initial phenol concentrations at pH 2 (Panel A) and pH 5 (Panel B). *cis*-FA has the same degradation rate constant as *trans*-FA. Error bars represent  $\pm$  1 standard error propagated from standard errors in linear fitting to obtain the slope and  $j_{2NB}$ . Dotted line represents fitted regression to the  $j_{SA}$  data at pH 5.

## Section S2: Phenolic aqSOA mass yields determination

102

119

Ammonium sulfate (AS) is used as an internal standard for aqSOA quantification,<sup>6-9</sup> under the assumption that sulfate is quantitatively extracted and measured by the AMS (a reasonable assumption given that the ammonium sulfate used is water soluble and non-refractory).<sup>10</sup> Thus, knowing the solution concentration of sulfate, we can use the AMS-measured concentration of ammonium sulfate in aerosols (AS<sub>AMS</sub>; μg m<sup>-3</sup>) to convert the AMS-measured aqSOA mass concentration (Org<sub>AMS</sub>; μg m<sup>-3</sup>) to solution concentration (mg L<sup>-1</sup>). The aqSOA yield is then given by:

$$SOA\ yield = \frac{[Org]_t - [Org]_0}{[phenol]_t - [phenol]_0} = \frac{[Org_{AMS}]_t \times \frac{[AS]_t}{[AS_{AMS}]_t} - [Org_{AMS}]_0 \times \frac{[AS]_0}{[AS_{AMS}]_0}}{[phenol]_t - [phenol]_0}$$
(S1)

- where [Org], [AS], and [phenol] refer to the solution concentrations (mg L<sup>-1</sup>) of aqSOA, sulfate, and the phenol under consideration, respectively. The subscripts t and 0 denote the irradiation time. As each sample was spiked to the same concentration of AS, [AS]<sub>t</sub> = [AS]<sub>0</sub>. The phenol concentrations were determined by HPLC.
- A collection efficiency (CE) of 1 was used in this study for AMS data processing. By using sulfate as an internal standard, the reported liquid aqSOA mass concentration is independent of CE and no correction is required. The reasons are 1) sulfate is expected to be quantitatively measured by the AMS<sup>10</sup> and 2) the aqSOA and sulfate are expected to be internally mixed in the aerosol generated from the reaction solutions.

## 120 **Section S3:** Phenol oxidation potentials determination

140

- 121 Cyclic voltammetry (CV) was performed using a three-electrode BASi EC Epsilon potentiostat consisting 122 of a 3-mm glassy carbon working electrode, an Ag/AgCl 3 M KCl reference electrode, and a 0.5 mm 123 diameter platinum wire (BASi) counter electrode. Before each set of measurements, the working electrode was polished with 0.05  $\mu$ m alumina polish. Cyclic voltammograms were recorded between -500 to 1200mV, 124 125 with scan speeds of 50, 100, and 200 mV/s. Measurements were performed in deoxygenated pH 2 (0.2 M 126 NaCl + 0.01 M HCl) and pH 5 (0.1 M potassium hydrogen phthalate + 0.04 M NaOH) buffer solutions with 127 0.25 mM of phenol. Since all phenols presented irreversible voltammograms, we report values of anodic peak potentials ( $E_p$ ) obtained directly from the voltammograms from the first scan (scan rate of 50 mV/s). 11 128 129 Potentials were corrected from the Ag/AgCl reference electrode to standard hydrogen electrode (SHE) by adding 209 mV.12 130
- Phenol oxidation potentials (for ArOH  $\rightarrow$  ArOH<sup> $\bullet^+$ </sup> +  $e^-$ ) were also calculated using Gaussian 09 software with procedures described previously. <sup>13,14</sup> Geometry optimization of phenols and phenoxyl radical cations were performed using uB3LYP functionals and 6-31+G(d,p) basis set. <sup>14–18</sup> Solvation energies were approximated with solvent mode density (SMD) continuum model for water. <sup>19</sup>
- The free energy of the reaction ( $\Delta G^{\circ}_{ox}$ ) was calculated by the difference in Gibbs free energy of the reactant and products, and was converted to one-electron oxidation potential ( $E_{OX}$ ) using:

$$E_{\rm OX} = -\left(\frac{-\Delta G^{\circ}_{\rm OX}}{nF} + {\rm SHE}\right) \tag{S2}$$

where *n* is the number of electrons (1 here), *F* is Faraday's constant (96485.3365 C mol<sup>-1</sup>), and SHE is the potential of the standard hydrogen electrode (4.28 V).<sup>20</sup>

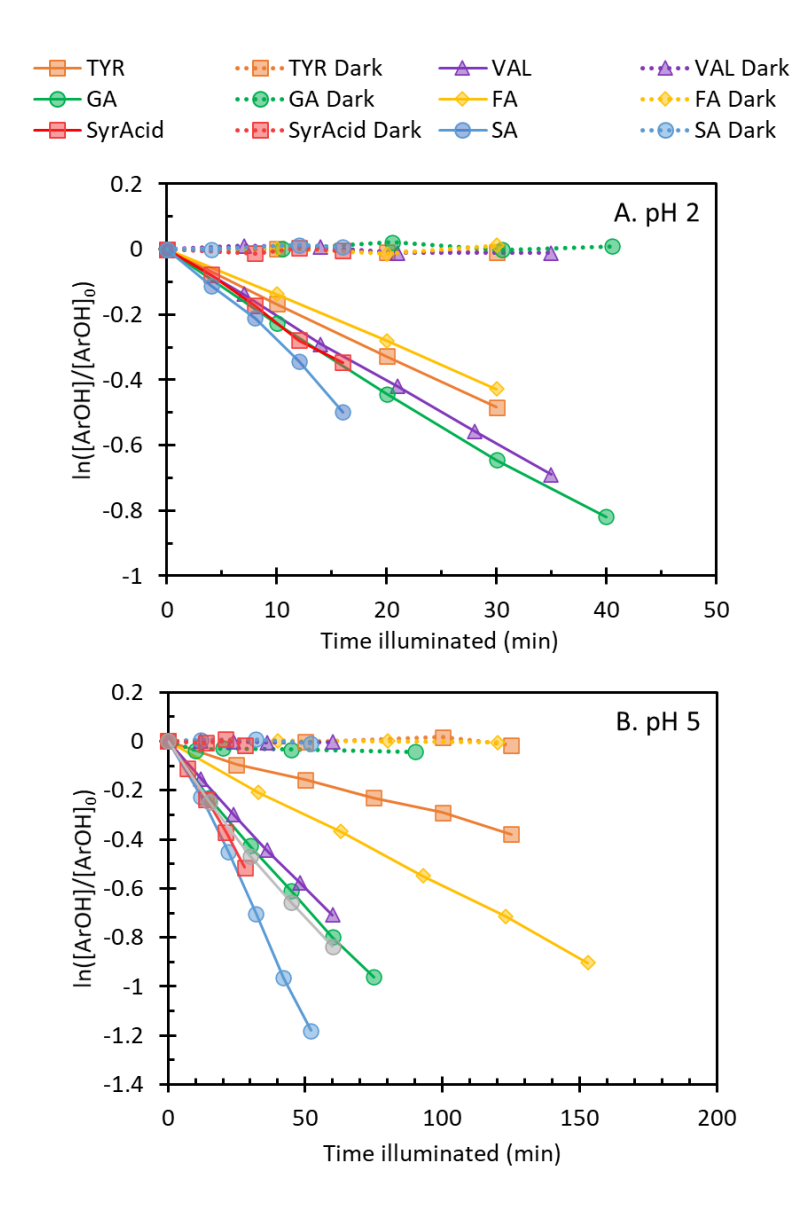


**Figure S2:** Representative plots of the aqueous oxidation of six phenols by the triplet excited state of DMB at pH 2 (Panel A) and pH 5 (Panel B) at 20 °C. Results shown here are for solutions containing 10  $\mu$ M ArOH and 10  $\mu$ M DMB. Solid lines represent the illuminated samples; dashed lines represent dark controls. The grey circles and corresponding line in the Panel B are data from the pH 5 oxidation of GA by  $^3$ DMB\* at 5 °C. These data are not statistically different from the 20 °C data (p < 0.05), indicating no significant impact of temperature on triplet kinetics, as seen previously for phenol ( $C_6H_5OH$ ) with triplet DMB. $^{21}$ 

### **Section S4:** Photoisomerization of ferulic acid

Ferulic acid isolated from plants usually exists as the *trans* isomer,<sup>22</sup> but during illumination it undergoes *cis-trans* isomerization to form a mixture of both isomers,<sup>23,24</sup> which can be separated by HPLC. The rate of FA photoisomerization is more rapid than that of reaction with <sup>3</sup>DMB\*: under our illumination conditions, 10  $\mu$ M FA reaches an isomeric photostationary state within 3 min (Figure S3). In experiments of FA reacting with <sup>3</sup>DMB\*, we removed aliquots for FA analysis at intervals greater than 10 min, thus photoisomerization should be at steady state. In our triplet experiments with FA, we first prepared a pH-adjusted solution containing *trans*-FA and illuminated it for 10 minutes to achieve photoisomerization steady state. Next, we added DMB and illuminated to determine the decay rate constant of FA by <sup>3</sup>DMB\*. At a given pH value, *trans*-FA and *cis*-FA show essentially the same first-order decay rate, as shown in Figure S4.

The *cis/trans* ratio in the photostationary state varies with pH. At pH 2, [*cis*]/[*trans*] is about 0.5, while at pH 5, [*cis*]/[*trans*] is around 6, which is similar to results from Kahnt *et al.*.<sup>23</sup> We found that the presence of DMB did not affect the [*cis*]/[*trans*] ratio in illuminated solution at either pH. The rate constant for 10  $\mu$ M *trans*-FA isomerization can be determined by illuminating *trans*-FA solution, and then determining how the *trans*-FA and *cis*-FA concentrations change with time. The rate constant of a reversible reaction can be calculated using:<sup>25</sup>

$$-(j_{trans\to cis} + \frac{j_{trans\to cis}}{K_{eq}})t = ln\left(\frac{\frac{[cis]_t}{K_{eq}} - [trans]_t}{\frac{[cis]_0}{K_{eq}} - [trans]_0}\right) = ln\left(\frac{C_t^*}{C_0^*}\right)$$
(S3)

where  $j_{\text{trans}\to\text{cis}}$  is the first-order rate constant of photoisomerization from *trans*-FA to *cis*-FA;  $K_{\text{eq}}$  is the equilibrium constant of photoisomerization, i.e., the [cis]/[trans] ratio at the photostationary state; t is illumination time; and [cis] and [trans] are concentrations of the two isomers at a given time. The first-order rate constant of photoisomerization from cis-FA to trans-FA can be calculated using:<sup>25</sup>

$$j_{cis \to trans} = \frac{j_{trans \to cis}}{K_{eq}}$$
 (S4)

Using the data in the Figure S3, we calculated  $C_t^*$  (i.e.,  $\frac{[cis]_t}{K_{eq}} - [trans]_t$ ) at each time point and then obtained  $j_{trans \to cis}$  from the slope of a linear fitting between  $ln(\frac{C_t^*}{C_0^*})$  and time. j values were normalized to the sunlight condition of the midday on winter solstice at Davis (i.e.  $j_{2NB} = 0.007 \text{ s}^{-1}$ ). At pH 2,

 $j_{trans \to cis}$  is 0.23 s<sup>-1</sup> while  $j_{cis \to trans}$  is 0.46 s<sup>-1</sup>. At pH 5,  $j_{trans \to cis}$  is 0.031 s<sup>-1</sup> which is around six times faster than  $j_{cis \to trans}$  (0.005 s<sup>-1</sup>).

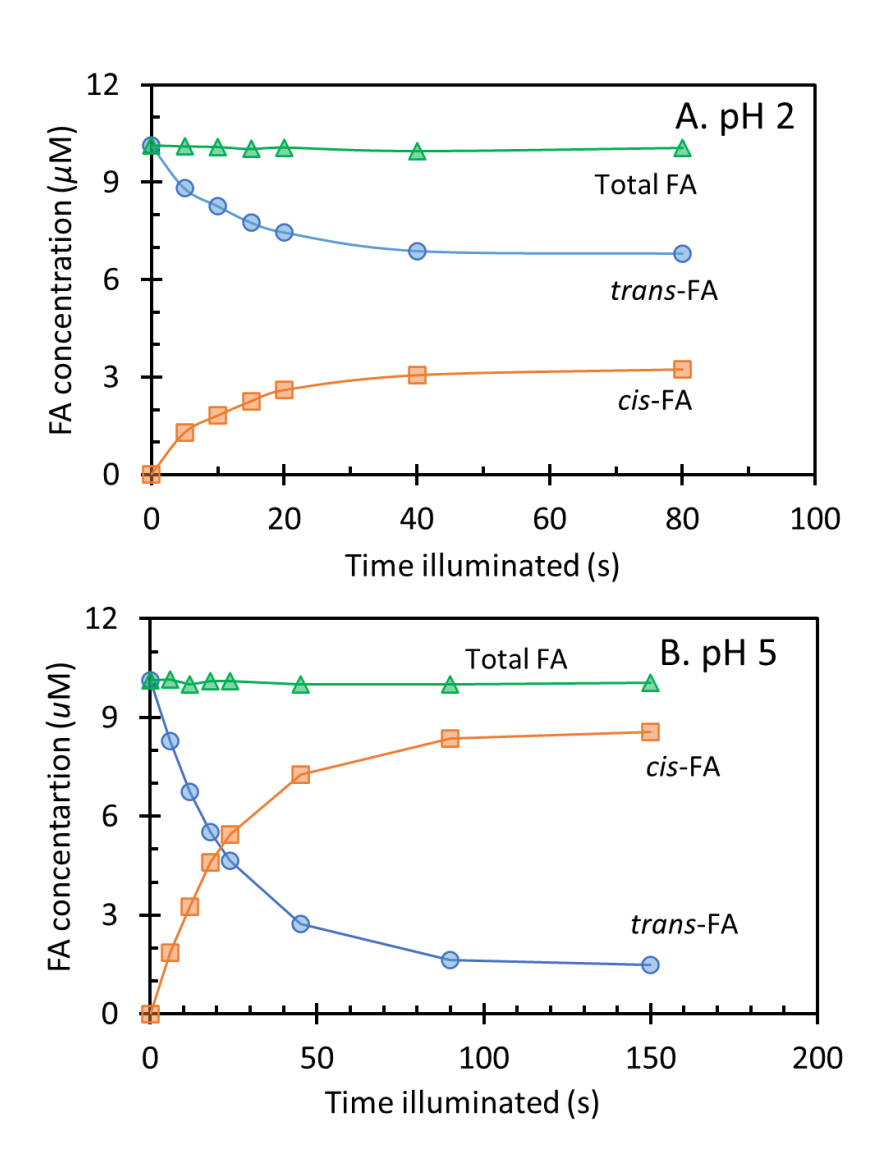


**Figure S3**: Changes in the concentrations of *trans*-FA (blue circles), *cis*-FA (orange squares), and total FA (*trans*-FA + *cis*-FA, green triangles) with illumination time during photoisomerization. The results shown here are for pH-adjusted solutions containing  $10 \, \mu M$  FA and no DMB.

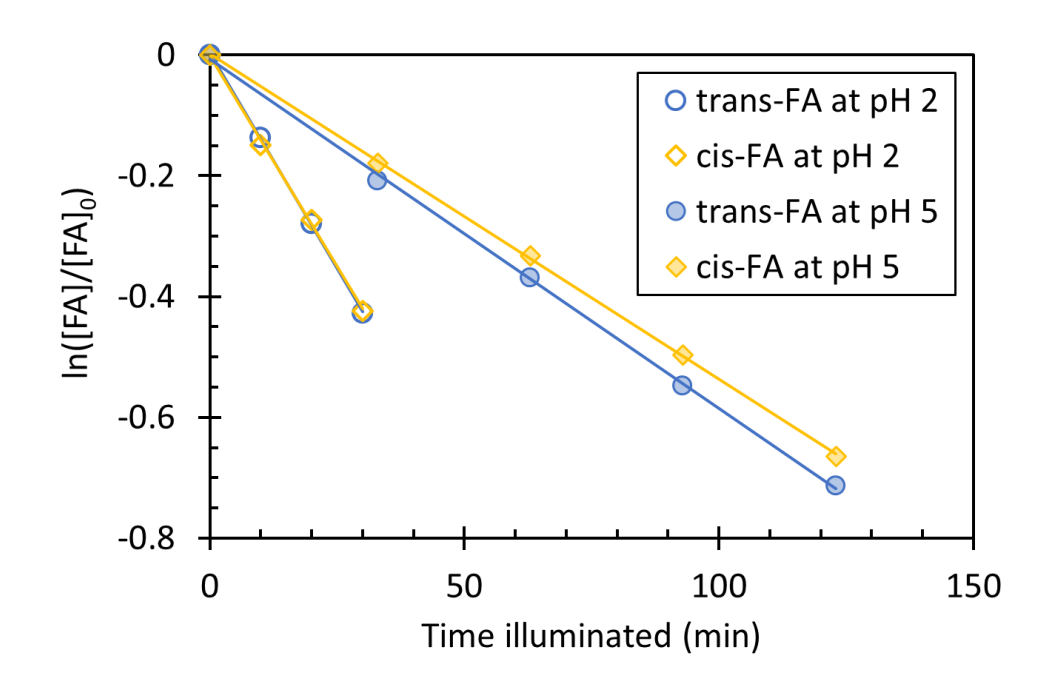


**Figure S4**: Representative plot of *trans*-FA (blue circle) and *cis*-FA (yellow diamond) decay with illumination time when reacting with  $^3$ DMB\* at pH 2 (open symbols) and pH 5 (filled symbols). Initial solutions contained 10  $\mu$ M total FA and 10  $\mu$ M DMB. Solid lines represent fitted regressions to the data.

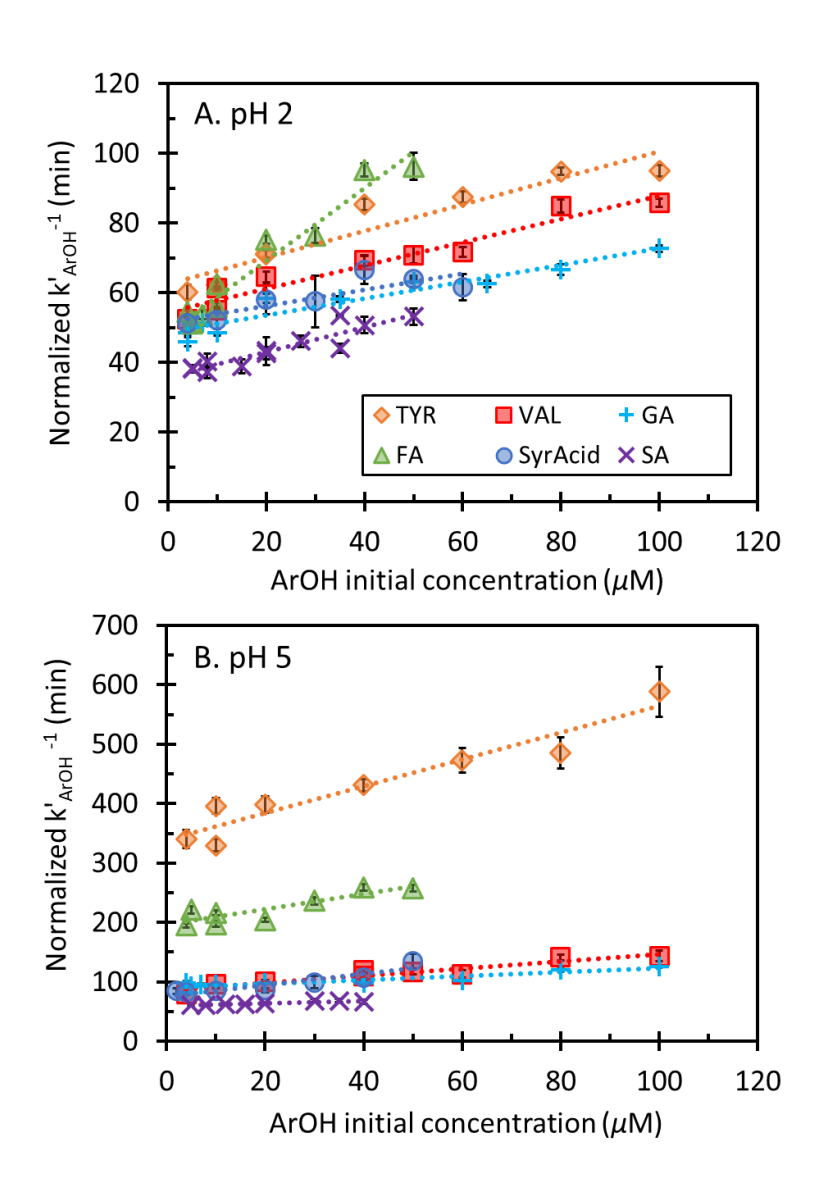


**Figure S5:** Inverse of the phenol first-order decay rate constant as a function of the initial phenol concentration at pH 2 (panel A) and pH 5 (panel B). Dotted lines represent fitted regressions to the data. Error bars on points represent  $\pm$  1 standard error propagated from the error of  $k'_{ArOH}$  (and  $j_{ArOH}$  for FA, SyrAcid, and SA).

**Table S3:** Regression parameters derived from plots of  $k'_{ArOH}$  versus ArOH initial concentration

	pI	H 2		pH 5			
	y-intercept <sup>a</sup> (min)	Slope <sup>a</sup> (min $\mu$ M <sup>-1</sup> )	$\mathbb{R}^2$	y-intercept <sup>a</sup> (min)	Slope a $(\min \mu M^{-1})$	$\mathbb{R}^2$	
TYR	62.48 (± 2.56)	$0.38 (\pm 0.05)$	0.91	339.2 (± 14.5)	$2.25 (\pm 0.28)$	0.92	
VAL	54.53 (± 1.75)	$0.33 (\pm 0.03)$	0.93	$86.16 (\pm 3.96)$	$0.61 (\pm 0.07)$	0.91	
GA	$48.70 (\pm 1.12)$	$0.24 (\pm 0.02)$	0.92	$89.99 (\pm 2.58)$	$0.33 \ (\pm \ 0.05)$	0.82	
trans-FA	$48.40 (\pm 1.94)$	$1.03 (\pm 0.08)$	0.95	$195.9 (\pm 7.59)$	$1.35 (\pm 0.30)$	0.78	
cis-FA	$48.63(\pm 2.14)$	$1.17 (\pm 0.09)$	0.95	$200.1 (\pm 11.7)$	$2.44 (\pm 0.44)$	0.83	
SyrAcid	$51.63 (\pm 2.39)$	$0.23~(\pm~0.07)$	0.71	$75.89 (\pm 5.08)$	$0.95 (\pm 0.18)$	0.85	
SA	35.82 (± 1.27)	$0.36 (\pm 0.05)$	0.85	$59.92 (\pm 0.94)$	$0.21 (\pm 0.04)$	0.83	

<sup>&</sup>lt;sup>a</sup>Regression parameters were determined by fitting the data in Figure S5 using Equation 3

**Table S4:** Second-order rate constants of phenols with <sup>3</sup>DMB\* at pH 2 and pH 5

		pH 2			pH 5	
	$k_{\text{ArOH+DMB}}^{\text{a}}$ (10 <sup>9</sup> M <sup>-1</sup> s <sup>-1</sup> )	$k_{\rm Q}^{\rm b}$ (10 <sup>9</sup> M <sup>-1</sup> s <sup>-1</sup> )	$f_{ m reaction}{}^{ m c}$	$k_{\text{ArOH+DMB}} = (10^9  \text{M}^{-1}  \text{s}^{-1})$	$k_{\rm Q}$ (10 <sup>9</sup> M <sup>-1</sup> s <sup>-1</sup> )	$f_{ m reaction}$
TYR	$2.6 (\pm 0.66)$	$2.2 (\pm 1.8)$	$0.54 (\pm 0.13)$	$0.48 (\pm 0.12)$	4.8 (± 1.8)	$0.09 (\pm 0.02)$
VAL	$3.0 (\pm 0.75)$	$1.9 (\pm 1.8)$	$0.62 (\pm 0.14)$	$1.9 (\pm 0.48)$	$3.7 (\pm 2.0)$	$0.34 \ (\pm \ 0.08)$
GA	$3.3 (\pm 0.83)$	$0.58 (\pm 1.6)$	$0.85 (\pm 0.19)$	$1.8 (\pm 0.45)$	$1.1 (\pm 1.1)$	$0.61 (\pm 0.16)$
trans-FA	$3.4 (\pm 0.85)$	$14 (\pm 5.7)$	$0.20~(\pm~0.04)$	$0.83~(\pm~0.21)^{\rm d}$	$4.6 (\pm 2.1)$	$0.16 \ (\pm \ 0.05)$
cis-FA	$3.4 (\pm 0.84)$	$16 (\pm 6.4)$	$0.18 (\pm 0.04)$	$0.82 (\pm 0.21)^{d}$	$8.9 (\pm 3.6)$	$0.08 \ (\pm \ 0.02)$
SyrAcid	$3.2 (\pm 0.80)$	$0.41 (\pm 1.7)$	$0.88 (\pm 0.31)$	$2.1 (\pm 0.55)^{d}$	$7.8 \ (\pm \ 3.8)$	$0.22 (\pm 0.06)$
SA	4.5 (± 1.1)	$3.4 (\pm 3.0)$	$0.57 (\pm 0.14)$	$2.7 (\pm 0.68)$	$0.07 (\pm 1.2)$	$0.98 (\pm 0.26)$

<sup>&</sup>lt;sup>a</sup> Rate constant for reaction, calculated using Equation 2 and y-intercept values in Table S3. Listed uncertainties (in parentheses) are ± 1 standard error propagated from the standard errors in regression fittings, intersystem crossing quantum yield, and light absorption rate of DMB.

<sup>&</sup>lt;sup>b</sup> Rate constant for non-reactive triplet quenching, calculated using  $k_Q = \frac{k_{ArOH+3DMB*}}{f_{reaction}} - k_{ArOH+3DMB*}$ .

Uncertainties in parentheses are  $\pm$  1 standard error propagated from standard errors of  $k_{ArOH+3DMB*}$  and  $f_{reaction}$ .

<sup>&</sup>lt;sup>c</sup> Fraction of ArOH-<sup>3</sup>DMB\* interactions that result in chemical reaction (i.e., loss of ArOH), calculated using Equation 7 and the value of the slope in Table S3. Errors represents 1 standard error, propagated from the standard errors in regression fittings, intersystem crossing quantum yield, and light absorption rate of DMB.

<sup>&</sup>lt;sup>d</sup> Apparent second-order rate constant at pH 5, i.e. the rate constant of the mixture of the ion (carboxylate) and neutral forms of the phenol. The calculation details on the rate constants of neutral and ion forms with  $^3\text{DMB*}$  at pH 5 are shown in Section S5. The resulting rate constants are:  $k_{\text{HFA+3DMB*}} = 2.2 \ (\pm 0.45) \times 10^9 \ \text{M}^{-1} \ \text{s}^{-1}$ ,  $k_{\text{FA-+3DMB*}} = 0.31 \ (\pm 0.36) \times 10^9 \ \text{M}^{-1} \ \text{s}^{-1}$ ,  $k_{\text{SyrCOOH+3DMB*}} = 1.8 \ (\pm 0.44) \times 10^9 \ \text{M}^{-1} \ \text{s}^{-1}$ , and  $k_{\text{SyrCOOH+3DMB*}} = 2.2 \ (\pm 0.64) \times 10^9 \ \text{M}^{-1} \ \text{s}^{-1}$ .

Section S5: Determination of  $k_{ArOH+3DMB}$ \* for the neutral and ion (carboxylate) forms of FA and SyrAcid at pH 5

FA and SyrAcid have carboxylic acid groups (with p $K_a$  values of 4.6 and 4.2, respectively)<sup>26</sup> that at pH 5 will partially deprotonate to form carboxylate ions. Therefore, the apparent reaction rate constants of FA and SyrAcid with <sup>3</sup>DMB\* at pH 5 represent the reactivity of a mixture of the neutral and carboxylate forms of the phenols:

$$k_{ArOH+T} = \alpha_{PhCOOH} \times k_{PhCOOH+T} + \alpha_{PhCOO-} \times k_{PhCOO-+T}$$
 (S5)

where PhCOOH represents the neutral form, PhCOO<sup>-</sup> is the carboxylate (i.e., ion) form,  $k_{\text{PhCOOH+T}}$  and  $k_{\text{PhCOO+T}}$  values are the second-order rate constants for each form with the neutral DMB triplet state (T), and  $\alpha$  represents the mole fraction of each phenol species. For our other phenols with the base structure of guaiacol (2-methoxyphenol), the ratios of the second-order rate constants at pH 5 to those at pH 2, where the DMB triplet is protonated, (i.e.  $k_{\text{ArOH+T}}/k_{\text{ArOH+HT}}$ ) have an average ( $\pm$  1  $\sigma$ ) value of 0.63 ( $\pm$  0.11). Therefore, we assume that FA, which also has the base structure of guaiacol, has the same ratio for its neutral form in order to estimate the value of  $k_{\text{HFA+T}}$ . We can then use this value, along with the mole fractions, in Equation S5 to determine the rate constant for the carboxylate form of FA,  $k_{\text{FA-+T}}$ . For syringic acid, which has a base structure of syringol (2,6-dimethoxyphenol), we use a similar assumption and the average ( $\pm$  1  $\sigma$ ) ratio of  $k_{\text{ArOH+T}}/k_{\text{ArOH+HT}}$  for phenols based on syringol of 0.57 ( $\pm$  0.07). Using this method, we calculated rate constants for the neutral and ion forms of FA and SyrAcid with <sup>3</sup>DMB\*; values are shown in the footnote of Table S4.

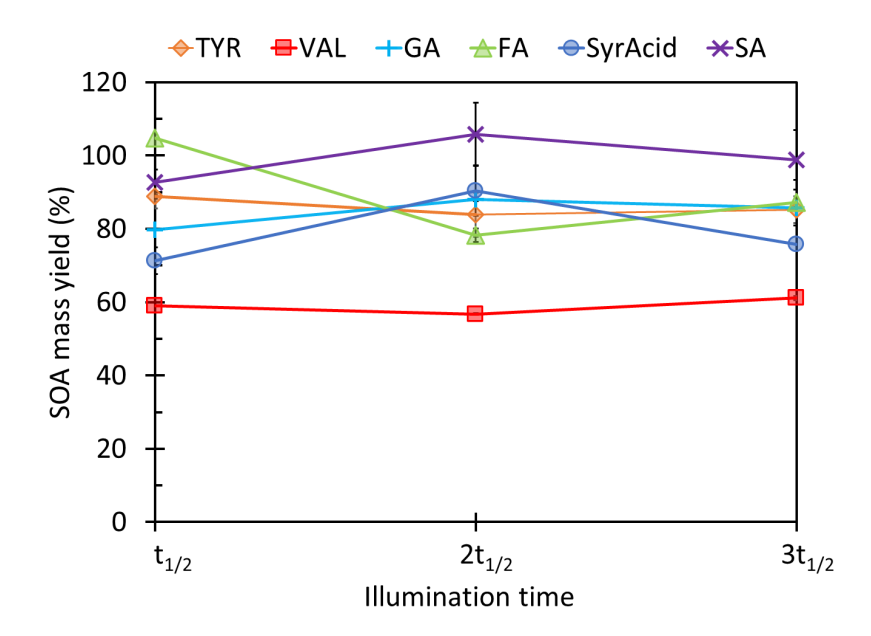


**Figure S6:** Time series of SOA mass yields during illumination, plotted at one, two, three half-lives of each phenol. Error bars are standard deviations of  $Y_{SOA}$  at each half-life from duplicate samples (except for FA at  $3t_{1/2}$ , where an outlier was removed and only one sample was available). In the calculation of the mean  $Y_{SOA}$  value for a given phenol shown in Figure 3,  $Y_{SOA}$  values at one, two, and three half-lives are used.

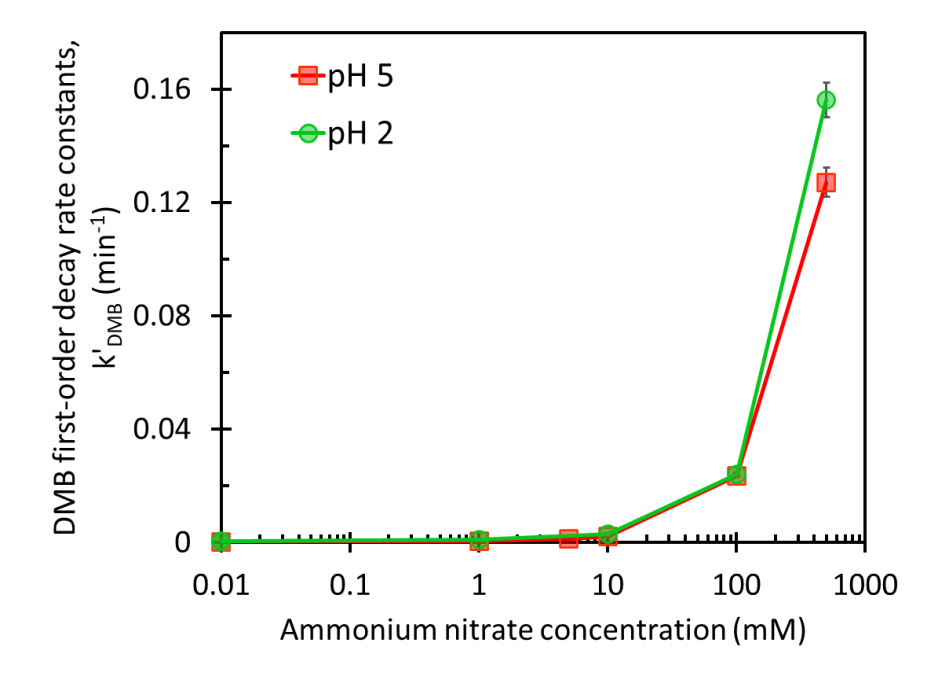


**Figure S7:** The dependence of the first-order rate constant of DMB decay on the concentration of ammonium nitrate at pH 5 and 2 after correcting for light screening due to nitrate. Since a zero value cannot be plotted on the logarithmic x-axis, we plot results for no added solutes (i.e., 0 mM ammonium nitrate) at a concentration of 0.01 mM. Error bars represent  $\pm$  1 standard error in  $k'_{DMB}$  determined from the linear regression fits. Data are not corrected for light screening by nitrate.

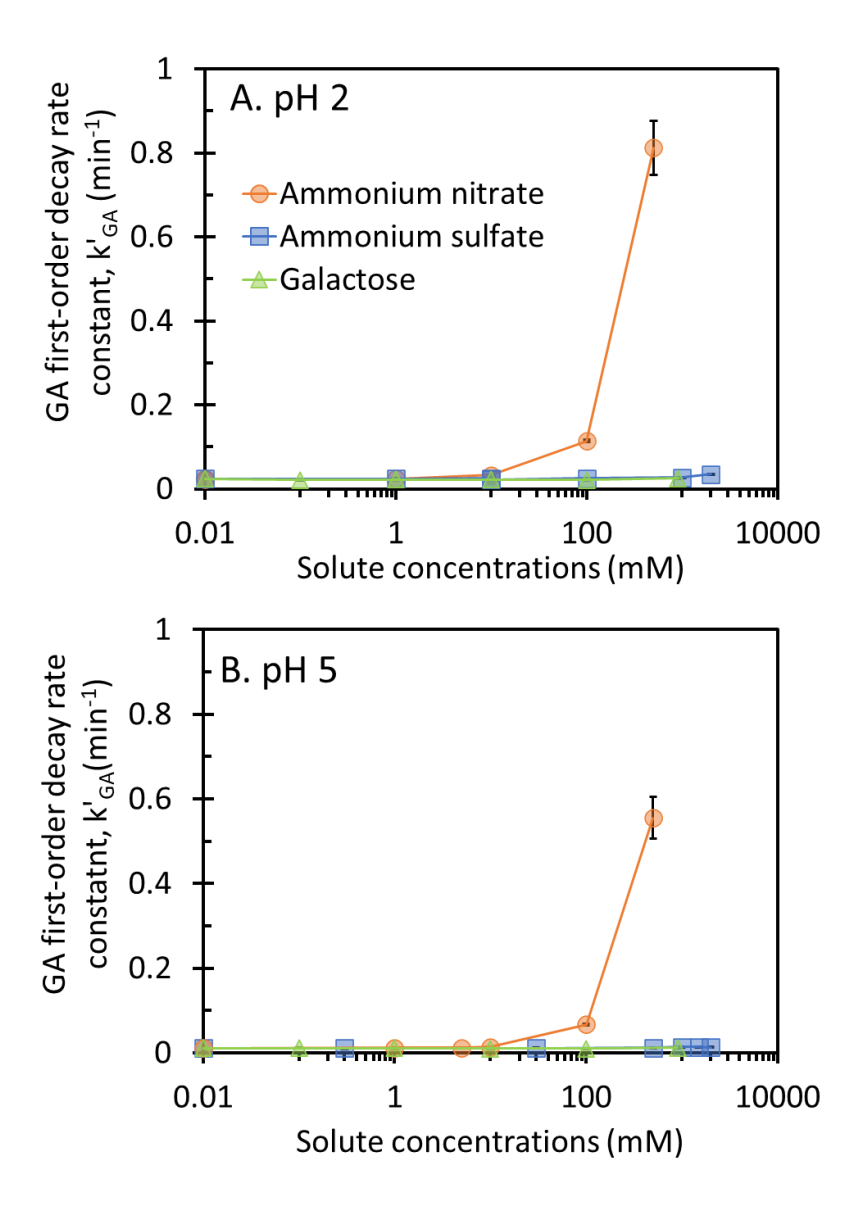


**Figure S8:** Dependence of the first-order rate constant of GA decay on the concentration of ammonium nitrate (orange circles), ammonium sulfate (blue squares), and galactose (green triangles) after correcting for light screening by nitrate. Since a zero value cannot be plotted on the logarithmic x-axis, we plot results for no added solutes at a solute concentration of 0.01 mM. Error bars represent  $\pm$  1 standard error in  $k'_{GA}$  from linear regression fits. The light screening factors for solutions containing 0, 1, 10, 100, and 500 mM nitrate are 0.85 (due to DMB light absorption), 0.84, 0.79, 0.45, and 0.15, respectively. A screening factor of 1 represents no screening, while smaller values indicate increasingly larger screenings.

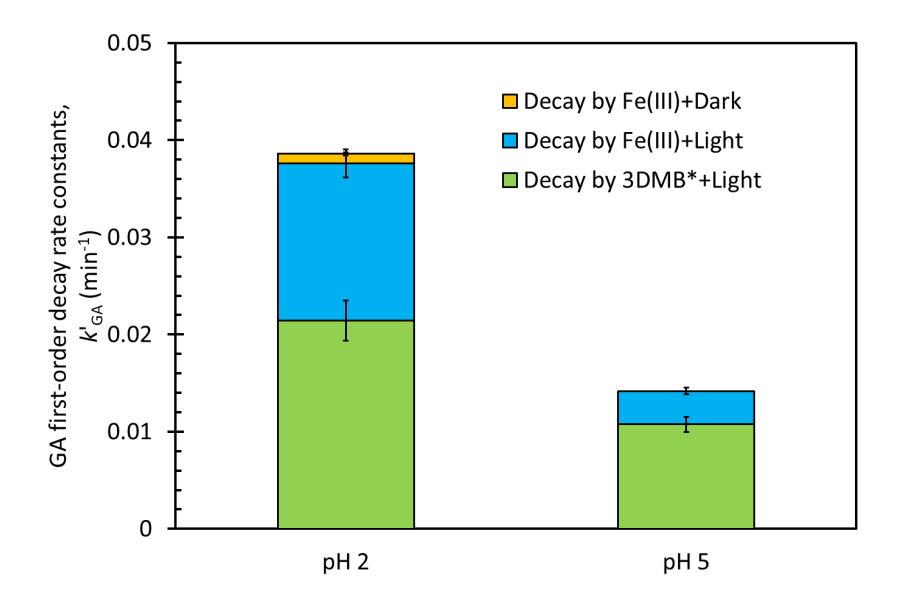


**Figure S9.** Decay of GA by  ${}^{3}$ DMB\* in the presence of Fe(III). The whole bars represent the total decay rates of GA in illuminated solutions containing both 20  $\mu$ M FeCl<sub>3</sub> and 10  $\mu$ M DMB. The yellow portion of the pH 2 bar is the dark decay of GA by Fe(III) in a solution with no DMB; the dark loss of GA in the presence of iron at pH 5 is negligible. The blue bars represent the decay rates of GA measured in illuminated solution containing 20  $\mu$ M FeCl<sub>3</sub> but no DMB. The green bars are the decay rates of GA by  ${}^{3}$ DMB\* after subtraction of its decay by Fe(III) under illumination and in the dark. Error bars represent  $\pm$  1 standard error in  $k'_{GA}$  from linear regression fits.

264
265

Commonada	Gaussian 09	Cyclic voltammetry		Suatoni et al. <sup>27</sup>	Pavitt et al. <sup>11</sup>	
Compounds		pH 2	pH 5	pH 5.6	pH 5.6	
Phenol	1.65	1.28	1.08	0.874	0.997	
Guaiacol	0.99	1.03	0.89	0.697	0.774	
Syringol	1.16	0.88	0.77	0.620	0.635	
Catechol	1.36	0.81	0.73		0.582	
Resorcinol	1.47	1.17	1.04		0.945	
Hydroquinone	1.17	0.73	0.63		0.509	
TYR	1.35	1.17	1.01			
VAL	1.16	1.01	0.83			
GA	1.07	1.00	0.84			
FA	1.26	1.02	0.78			
SyrAcid	1.39	1.06	0.78			
SA	0.99	0.86	0.72			

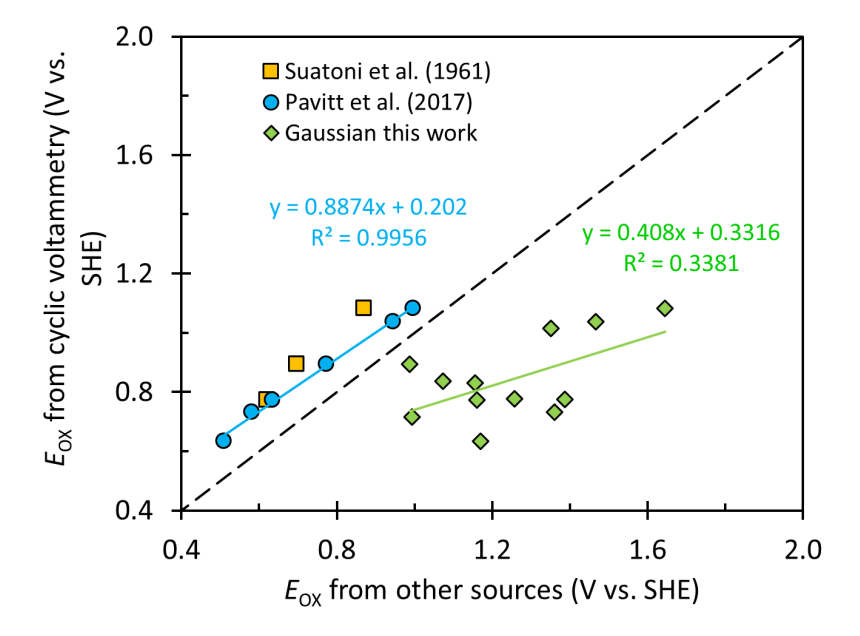


**Figure S10:** Comparison of our oxidation potentials measured using cyclic voltammetry with our computed values obtained from Gaussian and measured values from the literature. Since the oxidation potentials from Suatoni *et al.* and Pavitt *et al.* were measured at pH 5.6,<sup>11,27</sup> our CV values measured at pH 5 were used here for comparison. The solid green line represents the linear regression between our values of  $E_{OX}$  from CV and from Gaussian, with regression function next to it. The dashed line is the 1:1 line.

274 Section S6: Calculation of SOA formation rates from syringol, guaiacyl acetone, and syringyl acetone 275 To examine how gas- and aqueous-phase formation of SOA from phenols depends on liquid water 276 content (LWC), we calculated SOA formation rates for syringol (SYR), guaiacyl acetone (GA) and 277 syringyl acetone (SA) in a simple steady-state box model. We varied the LWC from 0.3 g m<sup>-3</sup> (representing a thick fog or cloud) to 1 µg m<sup>-3</sup> (representing a particle water condition) and assumed a 278 279 temperature of 278 K, Henry's law partitioning for the phenols, a particulate matter concentration of 10  $\mu$ g m<sup>-3</sup>, an initial concentration of an individual phenol of 5  $\mu$ g m<sup>-3</sup>, and an aqueous pH of 5. At each LWC 280 281 value we calculated the corresponding particle mass/water mass ratio and then used the corresponding measured/estimated steady-state aqueous oxidant concentrations (OH, 3C\*, 1O2\*) from Kaur et al.2; for 282 283 the triplet concentration at a given LWC we used the geometric mean value of the two estimates of Kaur et al. In the gas phase we considered ozone (30 ppbv) and  ${}^{\bullet}$ OH (1 × 10<sup>6</sup> molecule cm<sup>-3</sup>). Because rate 284 constants of ozone with phenols are quite slow, <sup>28</sup> O<sub>3</sub> was a negligible sink and we do not show its results. 285 286 As shown in Table S6, bimolecular rate constants of phenols with each oxidant ( $k_{ArOH+Ox}$ ) at pH 5, and the 287 corresponding SOA mass yields  $(Y_{SOA})$ , were obtained from literature when available. When there were no data available, we used data from phenols with a similar structure. Since no  $Y_{SOA}$  data are available for 288 289 phenols reacting with  ${}^{1}O_{2}*_{(aq)}$ , we assume this value to be 1, consistent with the high yields from other 290 aqueous reactions (Table S6). For each oxidant we would expect higher SOA mass yields at 5 °C 291 compared to 20 °C, because there would be less evaporation of semi-volatile organics. However, 292 we cannot experimentally assess the temperature effect on agSOA mass yields, we use the value 293 of Y<sub>SOA</sub> at 20 °C in these calculations. We do not include the impact of copper on phenol oxidation kinetics or aqSOA formation since this effect is poorly understood and requires more study. 294 295 To calculate the initial SOA formation rate, first we calculated the concentrations of phenols in the gas 296 and aqueous phases as a function of liquid water content. The Henry's law constants ( $K_{\rm H}$ ) of SYR (2.5 × 297  $10^4$  M/atm), GA (9.1 ×  $10^6$  M/atm), and SA (6.1 ×  $10^8$  M/atm) at 278 K were calculated from measured

299 
$$K_{H,278K} = K_{H,298K} \times exp(\frac{\Delta H_{sol}}{R} \times (\frac{1}{298 K} - \frac{1}{278 K}))$$
 (S6)

Since there is no available  $\Delta H_{sol}$  value for SA, we assume it has the same value as SYR. We calculate F(aq), the fraction of each phenol present in the aqueous phase, using:<sup>31</sup>

 $K_{\rm H}$  at 298 K and the enthalpy of dissolution  $(\Delta H_{sol})$ :<sup>29–31</sup>

$$F(aq) = \frac{1}{1 + \frac{1}{T \times R \times LWC \times K_H}}$$
 (S7)

303 where LWC is in dimensionless units (L-aq / L-air), T is the temperature (278 K) and R is the gas constant 304 (0.08206 L-air atm mol<sup>-1</sup> K<sup>-1</sup>).

The concentration of the phenol in each phase was calculated with:

$$[ArOH]_{aq} = [ArOH]_{tot} \times F(aq)$$
 (S8)

$$[ArOH]_{gas} = [ArOH]_{tot} \times (1 - F(aq))$$
 (S9)

The initial rate of SOA formation from one phenol reacting with an oxidant was then calculated with:

$$R_{SOA(aq),ox} = k_{ArOH+Ox} \times [ArOH]_{aq} \times [Ox]_{aq} \times Y_{SOA(aq),Ox}$$
 (S10)

The gas-phase SOA formation rate was calculated with an analogous form of this equation.

312 **Table S6:** Gas-

311

313

314

315

316

317

318319

# **Table S6:** Gas- and aqueous-phase reaction rate constants and SOA mass yields for SYR, GA, and SA with the major oxidants

Compounds		Syringol	Syringyl acetone	Guaiacyl acetone	
Gas phase rate constants	•OH <sub>(g)</sub>	9.66E-11	9.66E-11 <sup>b</sup>	7.53E-11°	
Gas-phase rate constants, $k_{ArOH+Ox(g)}$ (cm <sup>3</sup> molec <sup>-1</sup> s <sup>-1</sup> )	Ref.	(Lauraguais et	(Coeur-Tourneur <i>et al.</i> , 2010) <sup>33</sup>		
Gaseous reaction SOA mass yield, Y <sub>SOA(g)</sub>	•OH <sub>(g)</sub>	0.32	0.32 <sup>b</sup>	0.47 °	
	Ref.				
	•OH <sub>(aq)</sub>	2.0E+10	2.0E+10 b	1.6E+10 °	
	Ref.	(Smith <i>et al.</i> , 2015) <sup>1</sup>			
Aqueous-phase rate constants,	<sup>1</sup> O <sub>2</sub> * <sub>(aq)</sub>	3.6E+07	3.6E+07 b	6.0E+06 °	
$k_{\text{ArOH+Ox(aq)}} (\text{M}^{-1} \text{ s}^{-1})$	Ref.	(Tratnyek and Hoigne, 1991) <sup>35</sup>			
	<sup>3</sup> C* <sub>(aq)</sub> <sup>a</sup>	3.5E+09	2.7E+09	1.8E+09	
	Ref.	(Smith et al., 2015) <sup>1</sup>	This work	This work	
	•OH <sub>(aq)</sub>	1.14	1.14 <sup>b</sup>	1.09 °	
	Ref.	(Smith <i>et al.</i> , $2014$ ) <sup>21</sup>			
Aqueous reaction SOA	<sup>1</sup> O <sub>2</sub> * <sub>(aq)</sub>	1 <sup>d</sup>	1 <sup>d</sup>	1 <sup>d</sup>	
mass yields, $Y_{SOA(aq)}$	Ref.	-	-	-	
- 50A(aq)	<sup>3</sup> C* <sub>(aq)</sub> <sup>a</sup>	0.83	0.99	0.85	
<sup>8</sup> For trialet excited states yo	Ref.	(Smith et al., 2014) <sup>21</sup>	This work	This work	

<sup>&</sup>lt;sup>a</sup> For triplet excited states we use <sup>3</sup>DMB\* as the model triplet.

<sup>&</sup>lt;sup>b</sup> Since literature data is not available for SA, we used the values from syringol.

<sup>&</sup>lt;sup>c</sup> Since literature data is not available for GA, we used values from guaiacol.

<sup>&</sup>lt;sup>d</sup> No literature data is available for the SOA mass yield from phenols with <sup>1</sup>O<sub>2</sub>\*, so we assumed a value of 1, consistent with the high yields for the other two aqueous oxidants.

## Section S7: Determination of intersystem crossing quantum yield

320

335

336

337

338

339

340

341

321 Smith et al. determined the intersystem crossing (ISC) quantum yield for DMB ( $\Phi_{\rm ISC}$ ), and explained the 322 method in their supplemental information. Because their quantum yield has a relatively large uncertainty 323 (with a relative standard deviation of 30%), which contributes to a large uncertainty in the derived 324 second-order rate constants, we used their method to make additional measurements of  $\Phi_{\rm ISC}$  and reduce its 325 uncertainty. Briefly, we illuminated solutions containing 5 – 200  $\mu$ M SYR and 10  $\mu$ M DMB at pH 5 in a 326 monochromatic illumination system using light of 313 nm to measure the SYR loss rate. Next, we did a linear fitting of the inverse of the rate of SYR loss  $(R_{SYR,L,exp}^{-1})$  versus the inverse of the initial SYR 327 concentration to obtain the rate of SYR loss at infinite concentration  $(R_{ArOH,L,\infty})$ , which is the inverse of 328 329 the y-intercept from the linear fitting. This rate is equal to the rate of triplet excited state formation  $(R_{3C^*,F})$ 330 times the fraction of triplet interacting with phenols that leads to the decay of phenols ( $f_{\text{reaction}}$ ). We use SYR as the model phenol because its value of  $f_{\text{reaction}}$  is essentially 1. Therefore,  $R_{\text{ArOH},L,\infty}$  essentially 331 332 equals the formation rate of the triplet excited state, allowing us to determine the ISC quantum yield 333 using:

$$\Phi_{\rm ISC} = \frac{R_{ArOH,L,\infty}}{2.303 \times \varepsilon_{313,DMB} \times l \times l'_{313} \times [DMB]}$$
 (S11)

where  $\varepsilon_{313,DMB}$  is the molar absorptivity of DMB at 313 nm, l is the cell pathlength, and  $l'_{313}$  is the actinic flux at 313 nm. This actinic flux was determined from  $j_{2\rm NB}$ , the decay rate constant of the actinometer 2-nitrobenzaldehyde (2-NB), which was measured on each experiment day. Results of our two new sets of experiments for the determination of  $R_{\rm ArOH,L,\infty}$  are shown in Figure S11. With Equation S11, we calculated  $\Phi_{\rm ISC}$  values of  $0.087 \pm 0.007$  and  $0.092 \pm 0.011$ . As shown in Table S7, we combined these data with results from Smith et~al. to determine an average ( $\pm~1\sigma$ ) value of  $\Phi_{\rm ISC}$  of  $0.095 \pm 0.017$ . This new average is very similar to the previously used value ( $0.10 \pm 0.03$ ) but has a smaller uncertainty.

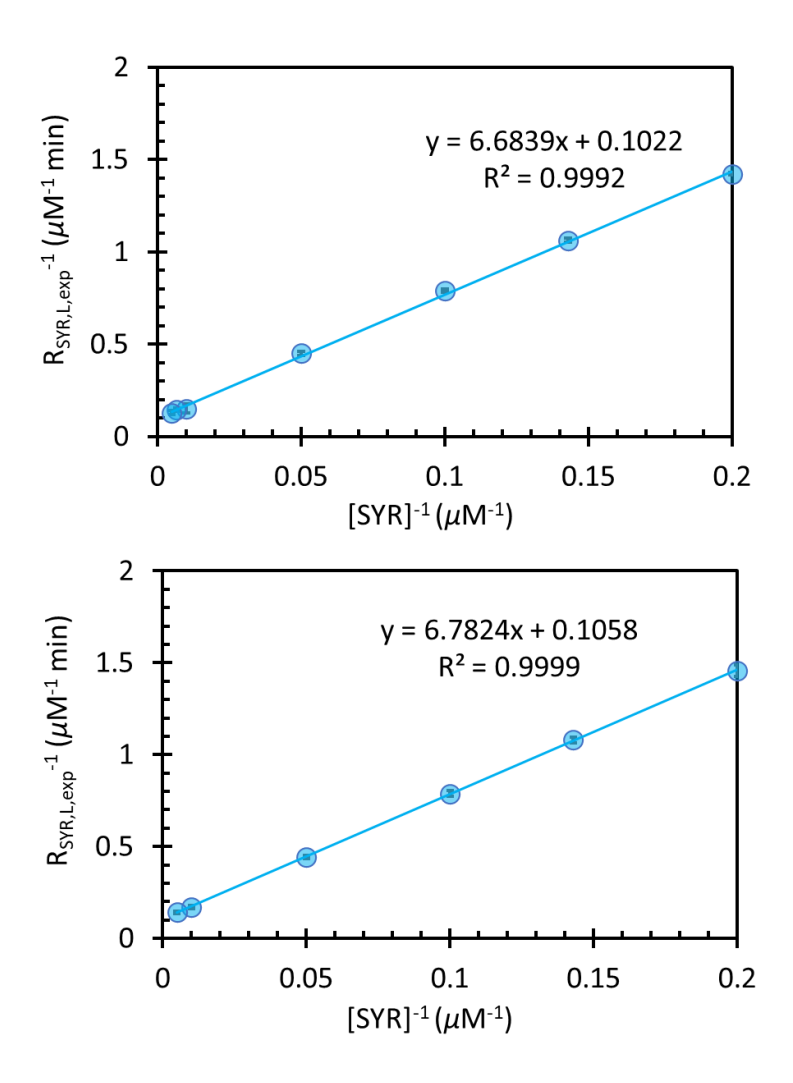


**Figure S11:** Experimental results of the decay of SYR reacting with  ${}^{3}DMB^{*}$  at 313 nm: the inverse of SYR loss rate versus the inverse of SYR initial concentration for two sets of independent experiments. The y-intercept is the inverse of the SYR loss rate at infinite SYR concentration. Error bars (which are smaller than the symbols) represent  $\pm 1$  standard error, propagated from standard errors in the linear fittings used to obtain  $R_{\text{SYR,L,exp}}$ .

**Table S7:** Summary of the quantum yield of <sup>3</sup>DMB\* intersystem crossing

	$\Phi_{ m ISC}$
Smith et al.1	$0.12~(\pm~0.01)^{\rm a} \ 0.08~(\pm~0.01)^{\rm a}$
This work	$0.087~(\pm~0.007)^{a}$ $0.092~(\pm~0.011)^{a}$
Mean $(\pm \sigma)$	0.095 (± 0.017) b

<sup>351</sup> 352 353

<sup>&</sup>lt;sup>a</sup> Standard error propagated from errors in  $R_{\text{SYR,L,}\infty}$ ,  $\varepsilon_{313,DMB}$ , and  $I'_{313}$  <sup>b</sup> Standard deviation of  $\Phi_{\text{ISC}}$  determined as the average of all four experiments

### REFERENCES

- Smith, J. D.; Kinney, H.; Anastasio, C. Aqueous benzene-diols react with an organic triplet excited state and hydroxyl radical to form secondary organic aerosol. *Phys. Chem. Chem. Phys.* **2015**, *17*, 10227–10237.
- Kaur, R.; Labins, J. R.; Helbock, S. S.; Jiang, W.; Bein, K. J.; Zhang, Q.; Anastasio, C.
   Photooxidants from brown carbon and other chromophores in illuminated particle extracts. *Atmos. Chem. Phys.* 2019, *19*, 6579–6594.
- 361 (3) Rounds, S. A.; Wilde, F. D.; Ritz, G. F. *Dissolved oxygen (ver. 3.0): U.S. Geological Survey*362 *Techniques of Water-Resources Investigations, book 9, chap. A6.2,*363 *https://doi.org/10.3133/twri09A6.2*; 09-A6.2; Reston, VA, 2006.
- 364 (4) Smith, J. D.; Kinney, H.; Anastasio, C. Phenolic carbonyls undergo rapid aqueous 365 photodegradation to form low-volatility, light-absorbing products. *Atmos. Environ.* **2016**, *126*, 36– 366 44.
- Jallin, E.; Wan, P.; Krogh, E.; Gill, C.; Moore, R. M. New pH-dependent photosubstitution pathways of syringic acid in aqueous solution: Relevance in environmental photochemistry. *J. Photochem. Photobiol. A* 2009, 207, 297–305.
- 370 (6) Yu, L.; Smith, J.; Laskin, A.; Anastasio, C.; Laskin, J.; Zhang, Q. Chemical characterization of SOA formed from aqueous-phase reactions of phenols with the triplet excited state of carbonyl and hydroxyl radical. *Atmos. Chem. Phys.* **2014**, *14*, 13801–13816.
- Huang, D. D.; Zhang, Q.; Cheung, H. H. Y.; Yu, L.; Zhou, S.; Anastasio, C.; Smith, J. D.; Chan,
   C. K. Formation and Evolution of aqSOA from Aqueous-Phase Reactions of Phenolic Carbonyls:
   Comparison between Ammonium Sulfate and Ammonium Nitrate Solutions. *Environ. Sci. Technol.* 2018, 52, 9215–9224.
- 377 (8) Sun, Y. L.; Zhang, Q.; Anastasio, C.; Sun, J. Insights into secondary organic aerosol formed via aqueous-phase reactions of phenolic compounds based on high resolution mass spectrometry.

  Atmos. Chem. Phys. 2010, 10, 4809–4822.
- Jiang, W.; Misovich, M. H.; Anusha Priyadarshani Silva; McFall, A.; Anastasio, C.; Zhang, Q.
   Photosensitized Reactions of a Phenolic Carbonyl from Wood Combustion in the Aqueous Phase
   Chemical Evolution and Light Absorption Properties of AqSOA. *Environ. Sci. Technol.* 2021
   (in press).
- 384 (10) Daellenbach, K. R.; Bozzetti, C.; Křepelová, A.; Canonaco, F.; Wolf, R.; Zotter, P.; Fermo, P.; 385 Crippa, M.; Slowik, J. G.; Sosedova, Y.; Zhang, Y.; Huang, R. -J.; Poulain, L.; Szidat, S.; 386 Baltensperger, U.; EI Haddad, I.; Prévôt, A. S. H. Characterization and source apportionment of organic aerosol using offline aerosol mass spectrometry. *Atmos. Meas. Tech.* **2016**, *9*, 23–39.
- 388 (11) Pavitt, A. S.; Bylaska, E. J.; Tratnyek, P. G. Oxidation potentials of phenols and anilines: correlation analysis of electrochemical and theoretical values. *Environ. Sci. Process. Impacts* **2017**, *19*, 339–349.
- 391 (12) Zoski, C. G. ed., *Handbook of Electrochemistry*; Elsevier, 2007.
- Frisch, M. J.; Trucks, G. W.; Schlegel, H. B.; Scuseria, G. E.; Robb, M. A.; Cheeseman, J. R.; Scalmani, G; Barone, V.; Petersson, G. A.; Nakatsuji, H.; Li, X.; Caricato, M.; Marenich, A.;
- Bloino, J.; Janesko, B. G.; Gomperts, R.; Mennucci, B.; Hratchian, H. P.; Ortiz, J. V.; Izmaylov,
- A. F.; Sonnenberg, J. L.; Williams-Young, D.; Ding, F.; Lipparini, F.; Egidi, F.; Goings, J.; Peng,

- B.; Petrone, A; Henderson, T.; Ranasinghe, D.; Zakrzewski, V. G.; Gao, J.; Rega, N.; Zheng, G.;
- Liang, W.; Hada, M.; Ehara, M.; Toyota, K.; Fukuda, R.; Hasegawa, J.; Ishida, M.; Nakajima, T.;
- Honda, Y.; Kitao, O.; Nakai, H.; Vreven, T.; Throssell, K.; Montgomery, J. A.; Peralta, Jr., J. E.;
- Ogliaro, F.; Bearpark, M.; Heyd, J. J.; Brothers, E.; Kudin, K. N.; Staroverov, V. N.; Keith, T.;
- Kobayashi, R.; Normand, J.; Raghavachari, K.; Rendell, A.; Burant, J. C.; Iyengar, S. S.; Tomasi,
- J.; Cossi, M.; Millam, J. M.; Klene, M.; Adamo, C.; Cammi, R.; Ochterski, J. W.; Martin, R. L.;
- 402 Morokuma, K.; Farkas, O.; Foresman, J. B.; Fox, D. J. Gaussian 09, Revision A.02. *Gaussian*,
- 403 *Inc.*, **2009**.
- 404 (14) Kaur, R.; Hudson, B. M.; Draper, J.; Tantillo, D. J.; Anastasio, C. Aqueous reactions of organic triplet excited states with atmospheric alkenes. *Atmos. Chem. Phys.* **2019**, *19*, 5021–5032.
- 406 (15) Lee, C.; Yang, W.; Parr, R. G. Development of the Colle-Salvetti correlation-energy formula into a functional of the electron density. *Phys. Rev. B, Condens. Matter* **1988**, *37*, 785–789.
- 408 (16) Stephens, P. J.; Devlin, F. J.; Chabalowski, C. F.; Frisch, M. J. Ab Initio Calculation of
   409 Vibrational Absorption and Circular Dichroism Spectra Using Density Functional Force Fields. J.
   410 Phys. Chem. 1994, 98, 11623–11627.
- 411 (17) Tirado-Rives, J.; Jorgensen, W. L. Performance of B3LYP density functional methods for a large set of organic molecules. *J. Chem. Theory Comput.* **2008**, *4*, 297–306.
- 413 (18) Becke, A. D. Density functional thermochemistry. I. The effect of the exchange only gradient correction. *J. Chem. Phys.* **1992**, *96*, 2155 2160.
- 415 (19) Marenich, A. V.; Cramer, C. J.; Truhlar, D. G. Universal solvation model based on the 416 generalized born approximation with asymmetric descreening. *Journal of chemical theory and* 417 *computation* **2009**, *5*, 2447–2464.
- Tripkovic, V.; Björketun, M. E.; Skúlason, E.; Rossmeisl, J. Standard hydrogen electrode and potential of zero charge in density functional calculations. *Phys. Rev. B* **2011**, *84*, 115452.
- 420 (21) Smith, J. D.; Sio, V.; Yu, L.; Zhang, Q.; Anastasio, C. Secondary organic aerosol production from aqueous reactions of atmospheric phenols with an organic triplet excited state. *Environ. Sci.*422 *Technol.* **2014**, *48*, 1049–1057.
- 423 (22) Graf, E. Antioxidant potential of ferulic acid. Free Radic. Biol. Med. 1992, 13, 435–448.
- 424 (23) Kahnt, G. Trans-cis-equilibrium of hydroxycinnamic acids during irradiation of aqueous solutions at different pH. *Phytochemistry* **1967**, *6*, 755–758.
- 426 (24) Changenet-Barret, P.; Plaza, P.; Martin, M. M. Primary events in the photoactive yellow protein chromophore in solution. *Chem. Phys. Lett.* **2001**, *336*, 439–444.
- 428 (25) Benjamin, M. M.; Lawler, D. F. *Water Quality Engineering: Physical / Chemical Treatment Processes*; 1st ed.; Wiley, 2013; p. 912.
- 430 (26) Erdemgil, F. Z.; Şanli, N.; Özkan, G.; Barbosa, J.; Guiteras, J.; Beltran, J. L.
  431 Determination of pKa values of some hydroxylated benzoic acids in methanol—water binary
- mixtures by LC methodology and potentiometry. *Talanta* **2007**, 72, 489–496.
- 433 (27) Suatoni, J. C.; Snyder, R. E.; Clark, R. O. Voltammetric studies of phenol and aniline ring substitution. *Anal. Chem.* **1961**, *33*, 1894–1897.

- 435 (28) Zein, A. E.; Coeur, C.; Obeid, E.; Lauraguais, A.; Fagniez, T. Reaction Kinetics of Catechol (1,2-436 Benzenediol) and Guaiacol (2-Methoxyphenol) with Ozone. *J. Phys. Chem. A* **2015**, *119*, 6759–6765.
- 438 (29) Sagebiel, J. C.; Seiber, J. N.; Woodrow, J. E. Comparison of headspace and gas-stripping methods for determining the Henry's law constant (H) for organic compounds of low to intermediate H.

  440 Chemosphere 1992, 25, 1763–1768.
- 441 (30) McFall, A. S.; Johnson, A. W.; Anastasio, C. Air-Water Partitioning of Biomass-Burning Phenols and the Effects of Temperature and Salinity. *Environ. Sci. Technol.* **2020**, *54*, 3823–3830.
- 443 (31) Seinfeld, J. H.; Pandis, S. N. *Atmospheric Chemistry And Physics: From Air Pollution To Climate Change*; 3rd ed.; Wiley: Hoboken, New Jersey, 2016; p. 1152.
- 445 (32) Lauraguais, A.; Coeur-Tourneur, C.; Cassez, A.; Seydi, A. Rate constant and secondary organic 446 aerosol yields for the gas-phase reaction of hydroxyl radicals with syringol (2, 6-447 dimethoxyphenol). *Atmos. Environ.* **2012**, *55*, 43–48.
- 448 (33) Coeur-Tourneur, C.; Cassez, A.; Wenger, J. C. Rate coefficients for the gas-phase reaction of hydroxyl radicals with 2-methoxyphenol (guaiacol) and related compounds. *J. Phys. Chem. A* **2010**, *114*, 11645–11650.
- 451 (34) Yee, L. D.; Kautzman, K. E.; Loza, C. L.; Schilling, K. A.; Coggon, M. M.; Chhabra, P. S.; Chan,
   452 M. N.; Chan, A. W. H.; Hersey, S. P.; Crounse, J. D.; Wennberg, P. O.; Flagan, R. C.; Seinfeld, J.
   453 H. Secondary organic aerosol formation from biomass burning intermediates: phenol and
   454 methoxyphenols. Atmos. Chem. Phys. 2013, 13, 8019–8043.
- Tratnyek, P. G.; Hoigne, J. Oxidation of substituted phenols in the environment: a QSAR analysis of rate constants for reaction with singlet oxygen. *Environ. Sci. Technol.* **1991**, *25*, 1596–1604.